COMPUTER MODEL OF AN INJECTION LOCKED PULSED CO_2 LASER

THESIS

Allen M. Susie
Captain, US Army

AFIT/GE/ENP/90D-01

DEPARTMENT OF THE AIR FORCE
AIR UNIVERSITY
AIR FORCE INSTITUTE OF TECHNOLOGY
Wright-Patterson Air Force Base, Ohio

AFIT/GE/ENP/90D-01

(1)

COMPUTER MODEL OF AN INJECTION LOCKED PULSED CO_2 LASER

THESIS

Allen M. Susie
Captain, US Army

AFIT/GE/ENP/90D-01

Approved for public release; distribution unlimited

AFIT/GE/ ENP/90D-01

COMPUTER MODELING OF AN INJECTION LOCKED PULSED CO_2 LASER

THESIS

Presented to the Faculty of the School of Engineering
of the Air Force Institute of Technology
Air University
In Partial Fulfillment of the
Requirements for the Degree of
Master of Science in Electrical Engineering

Allen M. Susie, B.S.
Captain, US Army

December 1990

Preface

The purpose of the study was to develop an extremely user friendly computer code to simulate an injection locked pulsed CO_2 laser. The use of this program is most suited to the design of lidar applications.

The program was written under the BASIC language format for use on an IBM-PC/AT compatible. Unfortunately a version of BASIC, Microsoft's BASIC version 7.0, was not available until after most of the code was written. Microsoft's BASIC will allow program and data modules to reside in extended or expanded memory. This advantage would result in more longitudinal modes tracked, longer pulse times, and smaller interval sizes used in computations.

I wish to thank MAJ Stone for his efforts and understanding during my thesis.

Allen M. Susie

Table of Contents

	Page
Preface	ii
List of Figures	v
Abstract	vii
I. Introduction	1
Key Terms and Definitions	1
Purpose of the Work	2
Scope of the Work	2
II. Equations and Model	4
Model of the Physical Process	4
Cavity Lifetime - t_{CAV}	6
σ - Effective Radiative Cross Sectional Area	6
Transition Rates between States	7
W_s - Spontaneous Generation of Flux Density	8
Pump Rates for Each State and Pump Cycle	9
Degeneracy Ratio	9
Field Equations for Injected Signals	10
Comparison of Flux versus Field Equations in Steady State	12
Injected Field and Phase Equations	13
Runge-Kutta Integration and Multimode Operations	15
III. Modifications to Equations for Multimode Operations	18
Normalization	18
Line Shape Factor in the Flux Rate Equation	19
Absorption Losses	20
Assumptions Used With the Model	21
Default Conditions	21
IV. Computer Program Implementation Considerations	23
Machine Details and Considerations	23
Software Considerations	23
Nominal Analysis for Step Size and Number of Modes	28
Nominal Analysis for Pressure and Step Size	30
V. Literature Review	33
Lachambre's Approach	33
Tratt CO_2 Laser Injection Study	36
Siegman's Derivation	38
Cassard and Lourtioz Approach	40
Conclusion	41

Page

VI. Results 42

Validation 42
Effect of Injected Signal Power on Power Evolution . . 51
Behavior of Injected Signal at Various Detuning Angles 54

VII. Conclusion 58

Bibliography 59

Vita 60

List of Figures

Figure		Page
1.	Model of the Physical Process in the Laser Study	4
2.	Computation Algorithm for Runge-Kutta Approximation	17
3.	Model of the Laser Cavity Showing Mechanical Parameters	22
4.	Multimode Display for Nominal Conditions at 30 Cavity Lifetimes	25
5.	Multimode Display for Standard Conditions at 400 tCav	26
6.	Display at 18 tCav Scaled against the Sum Total Peak Power	26
7.	Same Conditions as Figure 5 Scaled Against Mode 1	27
8.	Multimode Display at Occurrence of Peak Gain	27
9.	Time Evolution Display	28
10.	Nominal Analysis for Number of Modes	28
11.	Differences in Peak Power and Total Energy	30
12.	Increase of Power due to Pressure	30
13.	Effect of Pressure on Allowable Step Size	31
14.	Mode Selection Region (5:761)	34
15.	Mode Selection for Low Powered Injection (5:760)	35
16.	Mode Locking For High Injection Power (5:760)	35
17.	Change in Power Evolution due to Injection (11:237)	36
18.	Injected Regime (11:248) ϕ is the detuning angle	38
19.	Dependence of Peak Power on Cavity Length	43
20.	Total Power Percentage due to Injection.	44
21.	Display for an Injected Signal 1 W/cm^2	45
22.	Effect on Phase for Varied Powers with a 12° Offset	46
23.	Phase Dependence on Injected Power with 12° Offset	46
24.	Injected Signal Near Mode 4	47
25.	Display for Injected Signal of 1 W/cm^2 (Mid Pulse)	47
26.	Multimode Display for Injected Signal near Mode 1.	48
27.	Multimode Display for Injected Signal near Mode 4.	49

Figure Page

28. Display of an Injected Signal near Mode 1 at 400 t_{CAV}. . . . 49
29. Injection for Same Conditions as Figure 27 near Mode 4 . . . 50
30. Injected Signal with Power of 5 KW/cm^2 near Mode 1 51
31. Display for Same Conditions as Figure 30 near Mode 4 51
32. Amplified Injected Power for Injected Signal Powers 52
33. Total Power for Various Injection Levels 53
34. Total Power Evolution in Mid Pulse 53
35. Peak Power as a Function of Detuning Angle in Degrees 54
36. Dependence of Injected Peak Power on Detuning Angle 55
37. Time of Total Peak Power 56
38. Injected Peak Power Time 56

Computer Model of an Injection Locked Pulsed CO_2 Laser

Chapter I Introduction

The purpose of this chapter is to define key terms and to detail the direction and scope of the work. This chapter is divided into three sections. The first section consists of the definitions used throughout the document. The second section details the purpose of the work effort. The final section states the scope of the work.

Key Terms and Definitions

With the discovery of the laser there have been continual attempts to increase the "spectral brightness" (11:229) of a laser for applications such as signal processing and lidar. To this end techniques using either passive or active cavity elements have been developed to isolate a single longitudinal mode in both continuous and pulsed laser systems (11:230). Although passive elements have useful applications in continuous systems their use in pulsed systems is difficult to control (11:230). The injection of an external signal has proved very successful (11:230). Injection mode locking is a technique where a single frequency signal is used to seed the active medium during the gain build-up period (11:238). The laser transitions in CO_2 gas lasers are due to changes in the molecular energy in the vibrational or rotational aspects of the molecule. CO_2 may transition in one of three bands; the Regular band, the Hot band, and the Sequence band. In the Regular band transitions the energy exchange between vibrational states is very rapid because of the near-resonant energy transfer (13:68). The energy in one aspect of excitation can be exchanged for another mode of excitation. For the purposes of this thesis the focus will be on the transition between the first asymmetric stretch mode and the first

symmetric stretch mode in the Regular Band (13:14) or the $00^0 1$ to $10^0 0$ 10.6 um transition.

Due to collisions between molecules and the effect of the movement of molecules inside of the cavity the stimulated emission cross section becomes broadened. At low pressures below 10 torr the effect is primarily due to Doppler shifts of the transition frequencies (13:59). Above 50 torr the collision processes dominate (12:147; 13:60). This is called collision broadening or pressure broadening. This model is limited to the pressure broadened regime.

Purpose of the Work

An injection locked laser delivers superior frequency isolation and stability. Frequency isolation is rec .ed for laser radar designs. The purpose of the work was to produce a user friendly computer model which provides a realistic simulation of an injection seeded pulsed CO_2 laser. The computer language chosen was QuickBASIC® to allow easy future modification. QuickBASIC cannot compute complex numbers in the manner of FORTRAN. This limitation is overcome by the separation of real and imaginary parts of wave equations. The program will develop results for a set of physical conditions. The model will not develop the set of input conditions required to produce a specific result.

Scope of the Work

The computer program requires less than 128 kilobytes to run, utilizes an EGA display, and does not require extended or expanded memory. The model is based on a point model of the laser. This model utilizes four rate equations for a four state laser. The rate equations describe the populations in the three upper states and the photon density of the natural longitudinal modes. The rate equations are normalized to eliminate the dependence of the rate equations on physical units. In addition, two equations describe the cavity detuning angle

and power evolution for an injected laser. The model ignores higher quantum levels and focuses on the P(20) transition. The number of longitudinal modes is limited to a frequency range of eight free spectral ranges higher or lower than the transition frequency. This is due to the size of video display. The video display depicts the evolution of the power, gain, and energy of any mode in comparison to either the most powerful mode or to the summed power and energy in the laser pulse. The injected mode display shows the injected phase as well.

Chapter II describes the model and basic rate equations. Chapter III describes the modifications of the basic model for multimode operations. Chapter IV details the considerations used in developing the computer model. Chapter V contains the literature review relevant to laser injection locking and Chapter VI is a discussion of the results.

Chapter II Equations and Model

This chapter explores the physical model on which the computer code is based. As part of this model the discussion will include a short description of the spontaneous emission term, W_s. The transition rates between states and the pump rates for those states are delineated. Cavity lifetime is defined. The injection field equation is presented. The expression for instantaneous phase and injected signal field change is derived in a manner similar to other works. A comparison between steady state flux and field equations verifies the validity of the mixed approach instead of using field equations exclusively as Lachambre did in his works (5:757).

Model of the Physical Process

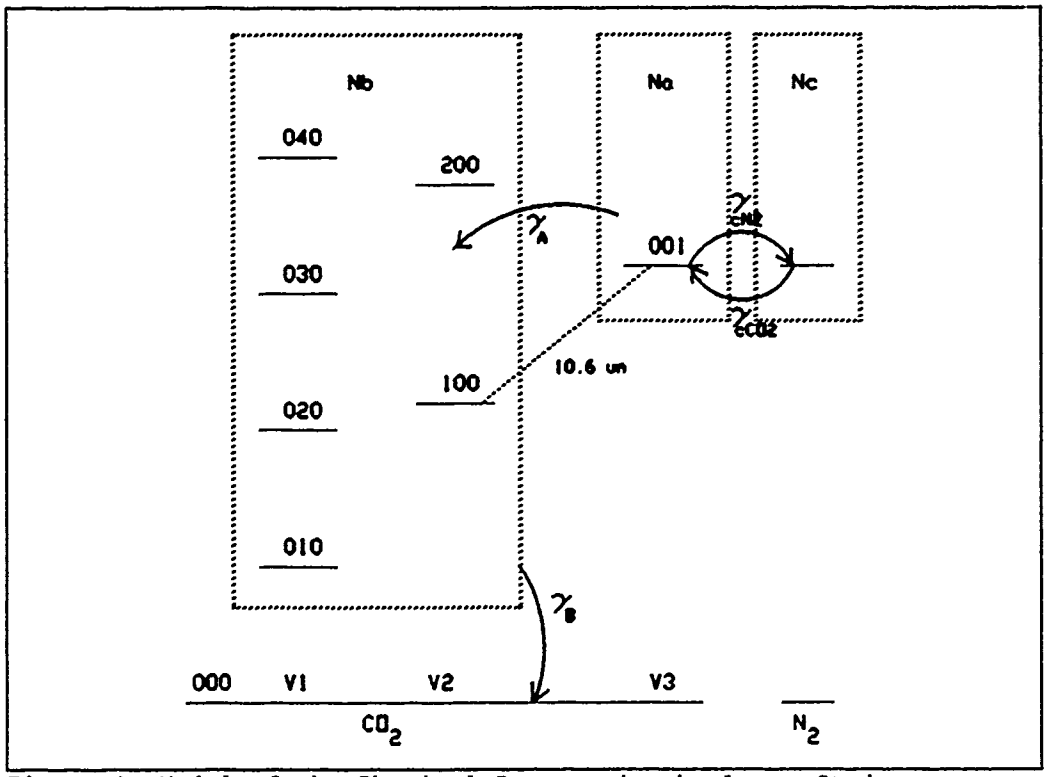

Figure 1 Model of the Physical Process in the Laser Study

The CO_2 laser process involved is the exchange of energy between the asymmetric stretch level of 00°1 and the symmetric stretch mode 10°0. Gilbert et al (3:2524) proposed a model of this process using the model shown as Figure 1. Figure 1 shows the existence of both the higher energy and lower energy states of CO_2 as well as the role of nitrogen as a reservoir of energy for the lasing process. The transition between nitrogen and carbon dioxide is endothermic. The higher carbon dioxide state is actually more energetic than that of the nitrogen by 18 cm^{-1} . This amount is small in comparison to room temperature energy - 208.3 cm^{-1} (12:261). The population rate equations that are applicable to this model are shown in equation set (1) (9:4).

$$\begin{aligned}
\frac{dN_a}{dt} &= \sigma c \psi (N_b - N_a) - \gamma_a N_a + \gamma_{cCO_2} N_c - \gamma_{cN_2} N_a + W_a \\
\frac{dN_b}{dt} &= \sigma c \psi (N_a - N_b) + \frac{\gamma_a}{4} N_a - \gamma_b N_b + W_b \\
\frac{dN_c}{dt} &= \gamma_{cN_2} N_a - \gamma_{cCO_2} N_c + W_c
\end{aligned} \tag{1}$$

The symbols follow the international system for units (S.I. units) unless otherwise noted: c is the speed of light, σ is the stimulated emission cross sectional area of the CO_2 molecule, ψ is the photon flux density in units, W_a, W_b, and W_c are the pumping rates for each population, and N_a, N_b, and N_c represent the concentrations of those populations. The γ symbols represent the collisional relaxation rates for the transitions between the states noted in Figure 1. The reduction by 1/4 in the equation for N_b is due to the fact that the transition from the higher to the lower energy state has a four different possible changes in state. Since we are interested in only one of these changes we incorporate this diversity by reducing the second term by 1/4. In addition, the rate equation for the photon density is shown in Eq (2):

$$\frac{d\psi}{dt} = \psi\sigma c\,(N_a - N_b) - \frac{1}{t_{CAV}}\psi + N_a W_s \qquad (2)$$

where t_{CAV} is the cavity lifetime and W_s is the term we will use to describe the spontaneous generation of flux in the manner of Gilbert (3:2525).

Cavity Lifetime - t_{CAV}

For the purposes of this work the cavity lifetime will be as shown in Eq (3) where L_{res} is the length of the cavity and R is the reflectivity of the output mirror with the assumption that the other mirror is lossless.

$$t_{CAV} = \frac{2L_{res}}{c}\frac{1}{\ln\left(\frac{1}{R}\right)} \qquad (3)$$

In some works (notably Lachambre), the cavity lifetime includes a factor for transmission losses or absorption losses inside the cavity itself. Lachambre defined the cavity lifetime as $t_{CAV} = 2\tau/[\ln(1/(RT)]$ where T is the transmissivity of the empty cavity and 2τ is the round trip time of a photon. T accounts for the internal losses of the cavity. Cavity losses affect the photon density on every trip through the cavity. An equivalent factor is possible. The photon density is reduced by an equivalent percentage for each time interval. This model will incorporate this concept in Chapter III.

σ - Effective Radiative Cross Sectional Area

The effect of pressure broadening is to reduce the effective radiative cross sectional area. This reduction also depends on the spectral separation from the laser transition. The effective radiative cross section of the molecule is Eq (4) (12:147; 13:57):

$$\sigma = \frac{\lambda_0^2}{8\pi} S(\nu_0, \nu) A_{coeff} \tag{4}$$

where λ_0 is the transition wavelength. The Einstein A coefficient, A_{coeff}, depends on the isotopes involved and is set at either 0.174 for C^{12} or 0.208 for C^{13} (4:534; 7:1091). The frequency for the transition has an isotope dependence; 28.306 THz for C^{12} and 26.889 Thz for C^{13} (13:23-49). The factor $S(\nu_0, \nu)$ designates the line shape and depends on frequency of the transition, ν_0, and the frequency of interest, ν. This factor is normalized according to Witteman (13:59) and Verdeyen (12:142) as Eq (5):

$$\int_0^\infty S(\nu_0, \nu) d\nu = 1 \tag{5}$$

The line shape is Lorentzian for high pressures. This results in Eq (6) (13:60) for line shape:

$$S(\nu_0, \nu) = \frac{\Delta\nu_p}{2\pi} \frac{1}{(\nu_0 - \nu)^2 + \left(\frac{\Delta\nu_p}{2}\right)^2} \tag{6}$$

The pressure broadening factor is taken from Witteman (13:61) shown in the next equation as:

$$\Delta\nu_p = 7.58 \left(\xi_{CO_2} + .73\,\xi_{N_2} + .64\,\xi_{He} + .38\,\xi_{H_2O} + .32\,\xi_{H2}\right) \times P \cdot 760 \sqrt{\frac{300}{T}} \text{ (in MHz)} \tag{7}$$

where ξ_{CO2}, ξ_{N2}, ξ_{He}, ξ_{H2O}, and ξ_{H2} refer to the fraction of the gas mix of that component (in total of 1), the pressure, P, is in units of atmospheres, and the temperature, T, is in Kelvin.

Transition Rates between States

The rates for the various transitions are dependent on the isotope of the carbon in the molecule, the gas pressure and the relative amounts

of each gas component. For C^{12} the set of rates from Lachambre (5:756) using the same notation as the previous equation is as follows (9:4):

$$\begin{aligned} \gamma_a &= P \cdot 760 \cdot (350\xi_{CO_2} + 106\xi_{N_2} + 85\xi_{He} + 24000\xi_{H_2O} + 3864\xi_{H_2}) \\ \gamma_{cN_2} &= P \cdot 760 \cdot 19100\xi_{N_2} \\ \gamma_{cCO_2} &= P \cdot 760 \cdot 17370\xi_{CO_2} \\ \gamma_b &= P \cdot 760 \cdot (194\xi_{CO_2} + 650\xi_{N_2} + 3270\xi_{He} + 450000\xi_{H_2O} + 71000\xi_{H_2}) \end{aligned} \tag{8}$$

The rates for the transitions for C^{13} are shown in Eq (9):

$$\begin{aligned} \gamma_a &= P \cdot 760 \cdot (1000\xi_{CO_2} + 304\xi_{N_2} + 90\xi_{He} + 24000\xi_{H_2O} + 3864\xi_{H_2}) \\ \gamma_{cN_2} &= P \cdot 760 \cdot 17370\xi_{N_2} \\ \gamma_{cCO_2} &= P \cdot 760 \cdot 19100\xi_{CO_2} \\ \gamma_b &= P \cdot 760 \cdot (194\xi_{CO_2} + 650\xi_{N_2} + 3270\xi_{He} + 450000\xi_{H_2O} + 71000\xi_{H_2}) \end{aligned} \tag{9}$$

The rates for the transitions for the lower state, γ_b, have been measured by an induced fluorescence technique where the molecules of a passive cell are excited and then spontaneously decay (13:76).

W_s - Spontaneous Generation of Flux Density

One can incorporate the effects of the Boltzmann distribution. The effective stimulated emission cross sectional area is a product of the stimulated emission cross sectional area and f_u, the thermal equilibrium probability of occupation (3:2535). The value of f_u is roughly 7% for the P(18) to P(22) transitions at standard temperature and pressure. For the P(19) transition the value of this reduction expressed as f_u is 0.0715 (3:2535). The spontaneous generation of flux depends on the product of the fraction of the molecules in the upper state, N_a, and W_s. W_s is a product of the inverse radiative lifetime of the lasing transition (the Einstein A coefficient) and the fraction of photons that are radiated into the small aperture of the secondary mirror within the spectral width of the axial mode, F (3:2523). The quantity F is shown in Eq (10) in derivation:

$$
\begin{aligned}
W_s &= F\, A_{coeff} \\
&= \frac{\lambda^2 f_u}{Area} S(\nu)\, d\nu\, A_{coeff} \\
&= \frac{\lambda_0^2 f_u}{Area} \frac{\Delta\nu_p}{2\pi} \frac{1}{(\nu-\nu_0)^2+\left(\frac{\Delta\nu_p}{2}\right)^2} d\nu\, A_{coeff} \\
&= \frac{\lambda_0^2 f_u}{Area} \frac{\Delta\nu_p}{2\pi} \frac{1}{(\nu-\nu_0)^2+\left(\frac{\Delta\nu_p}{2}\right)^2} \frac{1}{2\pi t_{CAV}} A_{coeff} \\
&= 4 \frac{\sigma}{Area\, t_{CAV}} \quad .
\end{aligned}
\tag{10}
$$

where Area is the area of the secondary mirror, $d\nu = 1/(2\pi\, t_{CAV})$, and $\Delta\nu_p$ is substituted from Eq (7).

Pump Rates for Each State and Pump Cycle

The model of this laser is not dependent on the pumping mechanism. This model does not incorporate any accounting for penetration depth or nonhomogeneous distribution of energies throughout the medium. Using the ideal gas law the pumping rate is calculated as follows in Eq (11) as:

$$
\begin{aligned}
W_c &= Eff_{pump}\, \xi_{N_2} \cdot 9.65 \cdot 10^{24} \cdot P \frac{760}{T \cdot \tau_{pump}} \\
W_a &= \frac{1}{3} Eff_{pump}\, \xi_{CO_2} \cdot 9.65 \cdot 10^{24} \cdot P \frac{760}{T \cdot \tau_{pump}} \\
W_b &= W_a
\end{aligned}
\tag{11}
$$

where the efficiency of the pumping mechanism is expressed as Eff_{pump}, and τ_{pump} is the length of the pump pulse. These equations incorporate the assumption that excitation of nitrogen is 3 times as effective as CO_2 and that the pumping is indiscriminate among the states (both N_a and N_b are equally pumped).

Degeneracy Ratio

The degeneracy ratio effects the small signal gain. This study assumes the P(20) transition is the only transition. P transitions have a rotational change of -1 (13:19). This rotational change from the

upper state, j', to the lower state, j, generates a degeneracy as $(2j'+1)/(2j+1) = g_u/g_l = 39/41 = 0.95122$ (13:63). Degeneracy impacts the stimulated transition term in Eq (2) as a factor reducing the amount of population in the upper state available to support the transition.

Field Equations for Injected Signals

For an amplified electromagnetic wave propagating in a cavity to have consistent boundary conditions the length of the resonator should be $n(\lambda/2)$ where n is any positive even integer. The wave builds without degradation due to inconsistent boundary conditions. Each wave exists on what we shall call a natural longitudinal mode. For an injected signal not on these resonance frequencies a phasor analysis is done. For such a field the signal at the end of a round trip (designated 2τ in time) we have:

$$\vec{E}_i(t+2\tau) = \text{gain}_{\text{roundtrip}}\,\vec{E}_i(t) + \vec{E}_0(t+2\tau) \tag{12}$$

where E_i is the evolving circulating signal and E_o is the injected signal. The round trip power gain of a cavity is G given by Eq (13):

$$G = T e^{\alpha(t) l} = g^2 \tag{13}$$

where T is the cumulative transmission gain ($0<T<1$) through the passive cavity for a round trip not including output coupling, $\alpha(t)$ is the power gain per unit length of amplifier and l is the length of the active section inside a cavity of length L_{res} becomes

$$\text{gain}_{(\text{round trip})} = g R e^{2jkL_{res}} \tag{14}$$

After the incorporation of Eqs (13) and (14), the round trip gain for any injected signal may be expressed as (10:395):

$$\text{gain}_{(\text{round trip})} \quad (RT)^{\frac{1}{2}} \exp\left[\frac{\alpha(t)\,l}{2} + 2j\,(kl_{res} - n\pi)\right] \tag{15}$$

where R is the product of the reflectivities of the mirrors in the optical path. The offset or detuning angle is the difference between a nearest natural mode and the injected signal. This is the difference between $2kL_{res}$ where k is the wave number of the injected signal and $2n\pi$ where n is an integer large enough to make the difference to a range of values between $-\pi$ and π. We will designate this difference as $d\theta$ (10:387). We convert the effects of the reflectivity and transmission losses from Eq (13). Next we take the natural logarithm to each side of Eq (15). We note that 2τ is equal to 2 * L_{res}/c. After dividing by 2τ an expression for the exponential representation of the evolving field is Eq (16):

$$\frac{\ln(\text{gain}_{\text{roundtrip}})}{2\tau} = \left(\frac{-1}{2\,t_{CAV}} + \frac{c\,\alpha(t)\,l}{4\,L} + j\,\frac{c\,d\theta}{2L}\right) = m(t) \tag{16}$$

A differential equation for the behavior of this wave is then developed through a Taylor's expansion. The Taylor's expansion for e^x where $0<x<1$ as $e^x = 1 + x + x^2/2! + x^3/3! + \ldots$ When x is small the first two terms of the expansion are a sufficient approximation. For a small gain scenario the value of a circulating wave at the end of a round trip is (10:395-396):

$$\vec{E}_1(t+2\tau) = e^{2\tau\frac{d}{dt}}\vec{E}_1(t) \tag{17}$$

By defining g_{rt} as the round trip gain in Eq (18)

$$g_{rt} = e^{2\tau m(t)} \tag{18}$$

we replace the round trip gain in Eq (12) with Eq (18):

$$e^{2\tau\frac{d}{dt}}\vec{E}_i(t) = e^{2\tau m(t)}\vec{E}_i(t) + \vec{E}_o(t+2\tau) \tag{19}$$

Through manipulation and using the forementioned Taylor's expansion as an approximation we develop a differential equation for an evolving field as:

$$\frac{d}{dt}\vec{E}_i(t) \approx m(t)\vec{E}_i(t) + \frac{m(t)\vec{E}_o(t+2\tau)}{e^{2\tau m(t)}-1} \tag{20}$$

Comparison of Flux versus Field Equations in Steady State

The flux density rate equation is equivalent to the field equation in the steady state. The flux rate Eq (2) is now written as:

$$\frac{d\psi}{dt} = \frac{-1}{t_{CAV}}\psi + \sigma_e c(\Delta N)\psi \tag{21}$$

where the degeneracy factor g_u/g_l is incorporated as seen in Eq (22):

$$\Delta N = N_a - \frac{g_u}{g_l}\cdot N_b \tag{22}$$

From the field model just derived

$$\frac{dE}{dt} = m(t)E(t) + m(t)\frac{E_{spont}}{e^{2\tau m(t)}-1} \tag{23}$$

where E is the evolving field of the longitudinal mode and E_{spont} is a term for the spontaneous generation of the field. After subtracting the spontaneous terms the field equation is

$$\frac{dE}{dt} = m(t)E(t) \tag{24}$$

The steady state for the equation of m(t) for natural longitudinal modes with no offset angle m(t) is Eq (25):

$$m(t) = \frac{-1}{2t_{CAV}} + \frac{cl\alpha(t)}{4L} \tag{25}$$

With the power gain coefficient, $\alpha(t)$, as follows

$$\alpha(t) = \sigma_e(N_a - \frac{g_u}{g_l} \cdot N_b) \cdot \frac{2L}{l} \tag{26}$$

m(t) becomes

$$m(t) = \frac{\sigma_e \Delta N c}{2} - \frac{1}{2t_{CAV}} \tag{27}$$

The exponent in the field equation is dimensionless and any quantity may be used to define the field E. Therefore, defining the field as the square root of the flux density the derivative of the field is:

$$\frac{dE}{dt} = \frac{d\psi^{\frac{1}{2}}}{dt} = \frac{1}{2}\psi^{-\frac{1}{2}}\frac{d\psi}{dt} \tag{28}$$

Eqs (24) and (25) with Eq (28) simplify to:

$$\frac{d\Psi}{dt} = -\frac{1}{t_{CAV}}\Psi + c\sigma_e \Delta N \Psi \tag{29}$$

Thus, the two forms for photon density and field (21) and (24) are equivalent as expected. An injected signal requires a phasor analysis.

Injected Field and Phase Equations

This section relies on the derivation of two first order non-linear differential equations as published in Computer Modeling of Gas Lasers (10:395-400):

$$\vec{E}_o = E_o(t)\, e^{j\omega_o t} \tag{30}$$

Let the value of the injected signal be represented by the expression above. The previous argument showed in the slowly varying analysis when

the injected signal was not changing quickly in time, i.e. $E_o(t) \simeq E_o(t+2\tau)$:

$$\frac{d\vec{E}_i}{dt} = m(t)\vec{E}_i(t) + \frac{m(t)\vec{E}_o(t)}{e^{2\tau m(t)}-1} \tag{31}$$

The equation for the evolving injected field is divided into magnitude and phase:

$$\vec{E}_i(t) = |\vec{E}_i(t)|e^{j\theta(t)} \tag{32}$$

Eq (32) becomes after differentiating:

$$\frac{d\vec{E}_i}{dt} = \frac{d|E_i(t)|}{dt}e^{j\theta(t)} + |\vec{E}_i(t)|\frac{jd\theta(t)}{dt}e^{j\theta(t)} \tag{33}$$

This in turn is the instantaneous field represented below (10:395):

$$\frac{d\vec{E}_i}{dt} = \frac{d|E_i(t)|}{dt}e^{j\theta} + |\vec{E}_i(t)|\frac{jd\theta}{dt}e^{j\theta} \tag{34}$$

The value of m(t) in Eq (16) is treated by dividing the expression into real and imaginary parts so that m(t) = x + jy. The expression for m(t) is substituted into Eq (31). Euler's identity is used on the exponential term in Eq (31). With the additional notation for the new variables c and d seen in Eq (35)

$$\begin{aligned} x &= \frac{-1}{2t_{CAV}} + \frac{c\alpha(t)l}{4L} \\ y &= \frac{cd\theta}{2L} \\ c &= e^{2\tau x}\cos(2\tau y) - 1 \\ d &= e^{2\tau x}\sin(2\tau y) \end{aligned} \tag{35}$$

we can compare like terms and derive the same equations in literature for phase and magnitude (10:400).

$$\eta = \frac{|E_i|}{E_o}$$

$$\frac{d\eta}{dt} = x\eta + \frac{\cos\theta(xc+yd) - \sin\theta(xd-yc)}{c^2+d^2} \qquad (36)$$

$$\frac{d\theta}{dt} = y - \frac{1}{\eta}\,\frac{\sin\theta(xc+yd) - \cos\theta(xd-yc)}{c^2+d^2} \qquad (37)$$

The combination of Eqs (36) and (37) describes the evolution of an injected signal and like the population and flux equations previously detailed are coupled differential equations. However, Eqs (36) and (37) are nonlinear differential equations due to the transcendental terms for θ.

Runge-Kutta Integration and Multimode Operations

The fourth order Runge-Kutta method of integration is accurate to the fifth order of the binomial expansion. Numerical integration provides approximate solutions to differential equations. For all the populations and flux densities given t_o as a start of an interval of duration h:

$$N_a(t_o+h) = N_a(t_o) + \int_{t_o}^{t_o+h} f(N_a, N_b, N_c, \text{flux}, \text{time})\,dt \qquad (38)$$

The end value of any population or flux equation depends on the initial value of that variable and the effects of change induced on all of the variables during the interval. Eq (38) is applicable to the other populations and the flux density as well. A series of successive approximations in Taylor Series expansion becomes equation set (39) for a generic variable y that is a function of x and y:

$$y(t_o+h) = y(t_o) + \int_{t_o}^{t_o+h} f(x,y)\,dt$$

$$y(t_o+h) = y(t_o) + k$$

where k is found by approximation as follows:

$$\begin{aligned} k_1 &= hf_o \\ k_2 &= hf\left(x_o+\tfrac{1}{2}h,\ y_o+\tfrac{1}{2}k_1\right) \\ k_3 &= hf\left(x_o+\tfrac{1}{2}h,\ y_o+\tfrac{1}{2}k_2\right) \\ k_4 &= hf\left(x_o+h,\ y_o+k_3\right) \\ k &= \tfrac{1}{6}\left(k_1+2k_2+2k_3+k_4\right) \end{aligned} \qquad (39)$$

The values of the integrand are relatively insensitive to changes in other variables in small gain, small interval models. However, there are many potential longitudinal modes. If each mode is not selected in isolation from other modes we have designated an order or precedence. This is not the case in reality. Instead we must hold the populations constant for all the flux calculations. Each mode's flux builds in isolation from other modes, affected by the "instantaneous" population only. These individual fluxes are then summed to obtain a new total flux for population effects. At the next time step the integration of individual mode's flux is based on the previous flux of that mode and again summed. This process is shown in Figure 2. Thus, the flux for each mode is based on the instantaneous populations frozen in time. This method of integration is accurate to the fifth order of the power series expansion of the function used to describe the independent variable (1:492).

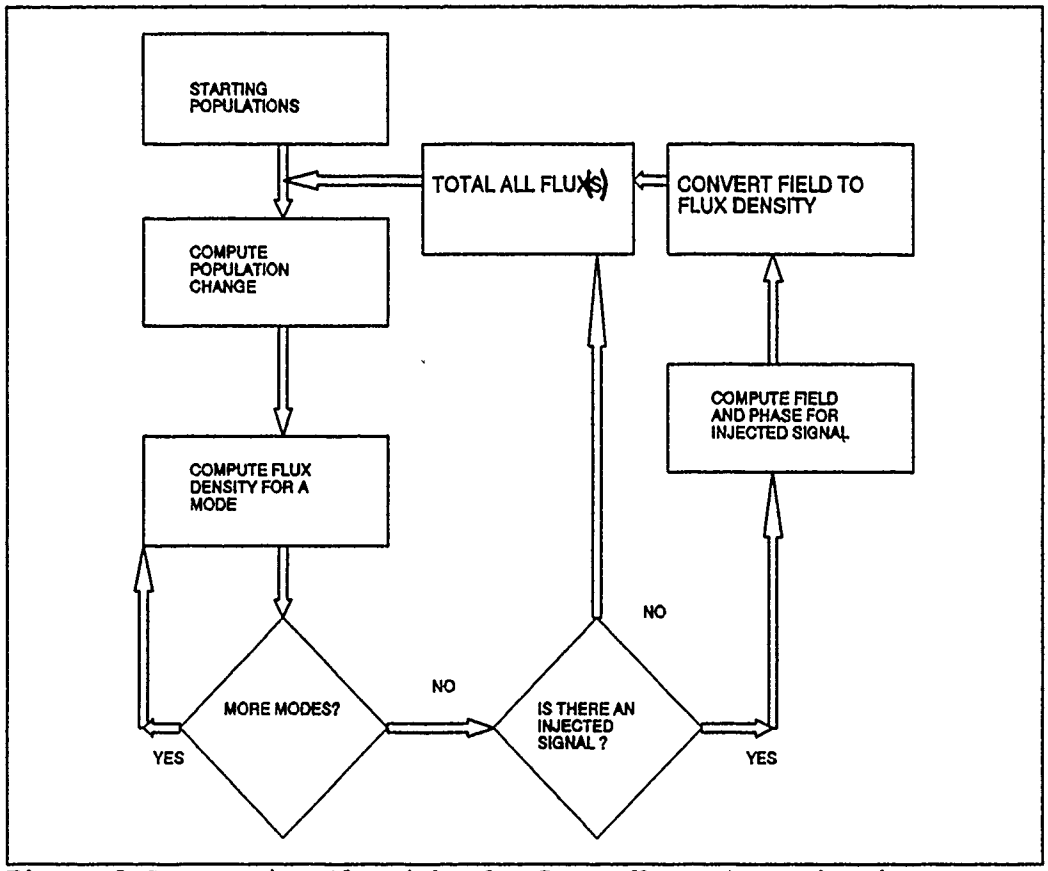

Figure 2 Computation Algorithm for Runge-Kutta Approximation

Chapter III Modifications to Equations for Multimode Operations

This chapter explains the extent to which the basic equations are modified for computer modeling. The first of these modifications is the normalization of the flux and population equations to dimensionless units. The second modification is the inclusion of the line shape factor in the flux equations to account for reduced cross sectional area due to frequency separation of the various longitudinal modes from the transition frequency. The assumptions inherent to the model and the simulation default settings are discussed.

Normalization

Normalization is a preferred technique that eliminates physical units from an equation or a system of equations. Additionally, normalization has the added benefit of eliminating computational problems involved in the Runge-Kutta technique. Without normalization, the chosen integration technique suffers a major error at the start of computations. The various populations are low in comparison to the decay rates and a negative population density develops. Although this effect can be countered by resetting the populations to zero density it is more practical to normalize. The electromagnetic field equation may be in any units desired. The equivalent expression for power in the photon rate equation is in units of photon density per second. The electromagnetic field is directly related to the square root of the power produced. As the power produced is directly related to photon density per second, the electromagnetic field equation defined in units of the square root of photon density per second is an equivalent expression as shown in Chapter II. The equations are normalized by choosing the critical photon density as the number of choice. This number, D_t, taken from Gilbert (3:2528) is $D_t=1/(tCav*\sigma_{center}*c)$ in meters^{-3}. The populations and flux variables are divided by D_t. Next

the pumping rates are multiplied by cavity lifetime, t_{CAV}, and divided by D_t. Finally, the transition rates are multiplied by t_{CAV}. This results in the series of equations shown as equation set (40) (3:2528).

$$\begin{aligned} \Phi &= \frac{\psi}{D_t} \\ n_{(a,b,c)} &= \frac{N_{(a,b,c)}}{D_t} \\ \Gamma_{(a,b,c)} &= \gamma_{(a,b,c)} \cdot t_{CAV} \\ w_{a,b,c,s} &= W_{(a,b,c,s)} \cdot \frac{t_{CAV}}{D_t} \end{aligned} \tag{40}$$

The complete equation set modified from Eqs (1) and (2) in Chapter II is shown as a matter of record as set (41) below.

$$\begin{aligned} \frac{dn_a}{dt} &= \Phi(n_b - n_a) - \Gamma_a n_a + \Gamma_{CO_2} n_c - \Gamma_{cN_2} n_a + w_a \\ \frac{dn_b}{dt} &= \Phi(n_a - n_b) + \frac{\Gamma_a}{4} n_a - \Gamma_b n_b + w_b \\ \frac{dn_c}{dt} &= \Gamma_{cN_2} n_a - \Gamma_{CO_2} n_c + w_c \\ \frac{d\Phi}{dt} &= \Phi(n_a - n_b) - \frac{1}{t_{CAV}} \Phi + n_a w_s \end{aligned} \tag{41}$$

Line Shape Factor in the Flux Rate Equation

Eqs (5) and (6) in Chapter II detailed the line shape factor for a homogeneously broadened condition. Recall that $S(\nu_0, \nu)$ was found to be:

$$S(\nu_0, \nu) = \frac{\Delta\nu_p}{2\pi} \frac{1}{(\nu_0 - \nu)^2 + \left(\frac{\Delta\nu_p}{2}\right)^2} \tag{42}$$

and that the effective radiative cross sectional area was found to be:

$$\sigma = \frac{\lambda_0^2}{8\pi} S(\nu_0, \nu) A_{coeff} \tag{43}$$

The formulation of the "line center" stimulated emission effective cross sectional area is derived by considering when $\nu = \nu_0$ exactly. When this condition is met $S(\nu_0, \nu) = 2/(\pi \Delta\nu_p)$ and so incorporating the distribution from Chapter II, Eq (10):

$$\sigma_{center} = \frac{f_u \lambda_0^2}{8\pi} \frac{2}{\pi \Delta \nu_p} A_{coeff} \tag{44}$$

This gives in turn an effective radiative cross sectional area, $\sigma_{effective}$, as seen in Eq (45):

$$\sigma_{effective} = \sigma_{center} \cdot \frac{\pi \Delta \nu_p}{2} \cdot S(\nu_0, \nu) \tag{45}$$

This factor, $\sigma_{effective}$, will be the factor, σ_e, used in the flux rate equations. Recalling that D_t incorporates σ_e, we must modify the cross sectional area in the flux equation to account for the frequency separation of the longitudinal modes.

Absorption Losses

The variable T in Eq (13) of Chapter II accounts for the transmission losses on a round trip basis. In accordance with the desire to account for "productive" output power the cavity lifetime described in Eq (3) of Chapter II does not account for those transmission losses in the cavity due to absorption. These losses in the cavity are accounted for by reducing the photon flux during each interval by an indexed amount for all the natural longitudinal modes. The injected signal will be degraded by an equivalent amount with the accounting for the difference between field and power. For the natural modes during a time period, t, for a cavity with a round trip time of 2τ and a distributed loss photon attenuation, β, the factor to multiply the flux density by is designated $Loss_{interval}$ as given by:

$$Loss_{interval} = 1 - \frac{t}{2\tau} \cdot \beta \tag{46}$$

$Loss_{interval}$ accounts for any size time period even if the interval is chosen to be very small order. The loss for the electromagnetic field of the injected signal at each round trip is simply:

$$loss_{interval} = 1 - \sqrt{\beta} \tag{47}$$

The interval size is forced to that of a round trip time when an injected field is studied and an indexed expression for field losses is not needed. This avoids a complicated equation set that would include accounting for positional field evolution of the injected signal in the cavity. Since this a point model of a laser, we will not force this derivation.

Assumptions Used With the Model

Spatial hole burning or inhomogeneity due to physical location is not considered. Another assumption is the lack of transition between nitrogen and ground state and the grouping of the other rates to include all transitions out of that state. In addition, in this point model the round trip gain must be smaller than one. This is due to the Taylor's expansion limitation on the argument described in Chapter II on page 11. As Gilbert (3:2525) explained these are reasonable assumptions if the length is short and the other physical assumptions previously described are valid.

Default Conditions

For further study a set of default conditions is required. A short description is given below. In addition to common physical constants for the speed of light and Planck's constant, the degeneracy ratio and the percentage of molecules in the P(20) transition are not changed throughout the simulation. The Einstein A coefficient is set for C^{12} at 0.174 sec^{-1}. The length of the resonator is 1 meter. The reflectivity is set to 71.636 percent. The area of the secondary mirror is 0.0004 square meters. The gain section has a gas mixture of 10% CO_2, 10% N_2, and 80% He confined at 1 atmosphere pressure at 300°K. The pump pulse is rectangular in shape, has an efficiency of 0.2 and the duration of the pump is 10 cavity lifetimes. The laser pulse output is tracked

to 400 cavity lifetimes. The cavity is not Q switched and nominal losses are 3%. During the pump pulse and until 30 cavity lifetimes the computational interval size is 0.1 cavity lifetimes. From 30 cavity lifetimes until 400 cavity lifetimes the interval size is 1 cavity lifetime. The normal number of longitudinal modes tracked is three. A schematic of the nominal model is shown in Figure 3.

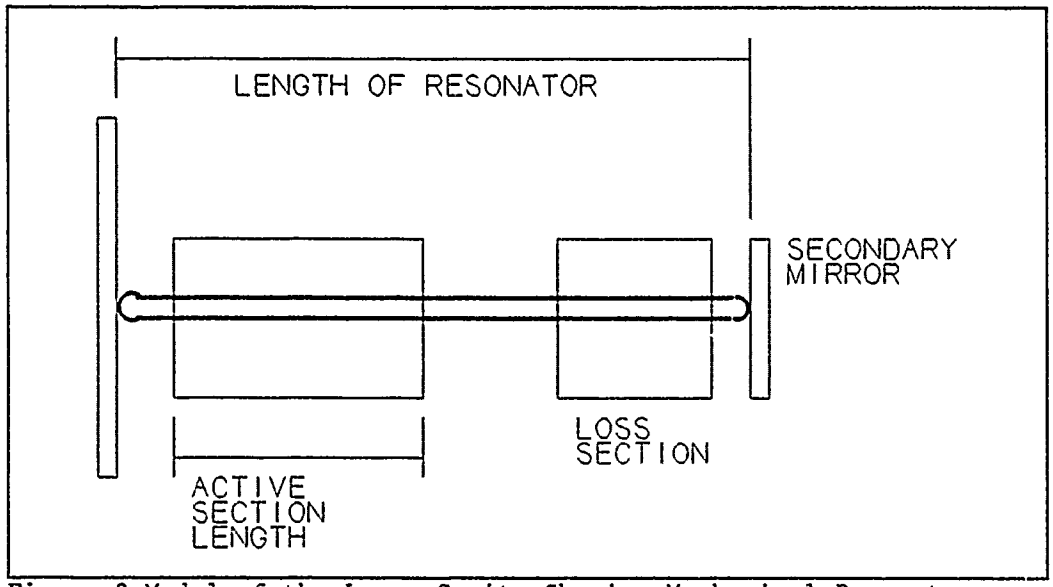

Figure 3 Model of the Laser Cavity Showing Mechanical Parameters

Chapter IV Computer Program Implementation Considerations

This chapter describes the computer on which the program was run. The software limitations are detailed. The display screens are described and examples provided. The program is exercised to determine the limits of a noninjected model in regards to pressure and computational step size.

Machine Details and Considerations

The program was written in QuickBASIC 4.5® for implementation on an IBM-PC® or compatible. The choice of language was not arbitrary - a previous effort tracking single mode operations was already available. The program compiles to a final size of 120 Kbytes. The computational run time is under three minutes using the standard defaults on a 25 Mhz 80386 based computer with a math coprocessor. The speed of execution depends largely on the number of side modes tracked, the various step sizes, and the length of time to track during the pulse process. A math coprocessor greatly speeds the time of execution.

Software Considerations

The program was written so that the majority of the variables were expressed in single precision format. This was based on the memory requirements for each type of precision - double precision representation requires 4 bytes to represent a number while single precision representation requires only 2 bytes. The program maintains in active memory at each time interval: the population of each state; the power, energy, and gain of each longitudinal mode; and the power, gain, energy, and the instantaneous phase angle of the injected signal. The simulation requires a significant amount of active memory for 16 modes (the maximum allowed) and a maximum interval size of 400 cavity lifetimes.

The computational routines are not the largest part of the program. The computations are mostly contained in one subroutine (RungeKutta4 for integration) with two function calls (differential equations: F for the populations and aModeflux for natural modes' flux). An additional subroutine is called for the computation of the instantaneous phase and for the computation of the change in the injected field strength. The majority of the program code generates a complex set of display screens and options that display the following normalized to the largest value of each category during the pulse or alternatively to the peak value of all the modes summed: (1) relative cross sectional areas; (2) the value of the injected signal cross sectional area relative to the cross sectional areas; (3) the evolution of the power, gain, and energy of any natural longitudinal mode (additionally phase for the injected signal); (5) the instantaneous power, gain, and energy profile of all modes at any time; (6) a numerical display of a mode's characteristics with population densities for any period of time; or (7) a numerical peak power and peak energy analysis. Gain curves on the graphs are always based on the highest gain by any single mode. An example of the display is shown in Figure 4. Figure 4 is a display of all of the modes at an instant of time. At the top left is the time in the pulse chosen for the display. The top right indicates that this particular graph is normalized to the peak values of the total power and total energy. Each individual mode has a group of three bars that chart the value of the particular field in comparison to the maximum total peak power, the maximum total energy, and the gain for the mode in comparison to the highest gain of any mode. At the right margin is a listing of the time of the maximum power of the most powerful mode, the time of maximum energy of the most powerful mode. the time of the peak gain of the most powerful mode, the time of the peak total power, and the time of the maximum energy. At the bottom

of the display is a listing of the arbitrary mode number. Mode numbers are assigned in order of increasing frequency separation from the transition frequency. Mode one is always the closest natural longitudinal mode to the transition frequency. The mode numbers are assigned alternatively with even numbers for progressively higher frequency natural longitudinal modes. Odd mode numbers are progressively lower in frequency. The display reinforces this with commentary notations at the bottom left and bottom right. Finally, the far right bar set is the total power and total energy at the same time as noted at the top left. Figure 4 shows this multimode display for an non-injected case. On the actual display the bars corresponding to power, gain, and energy are all in color. All individual power bars are blue, all gain bars are red, and energy bars are yellow. The total peak power and the maximum energy are depicted in purple and green respectively.

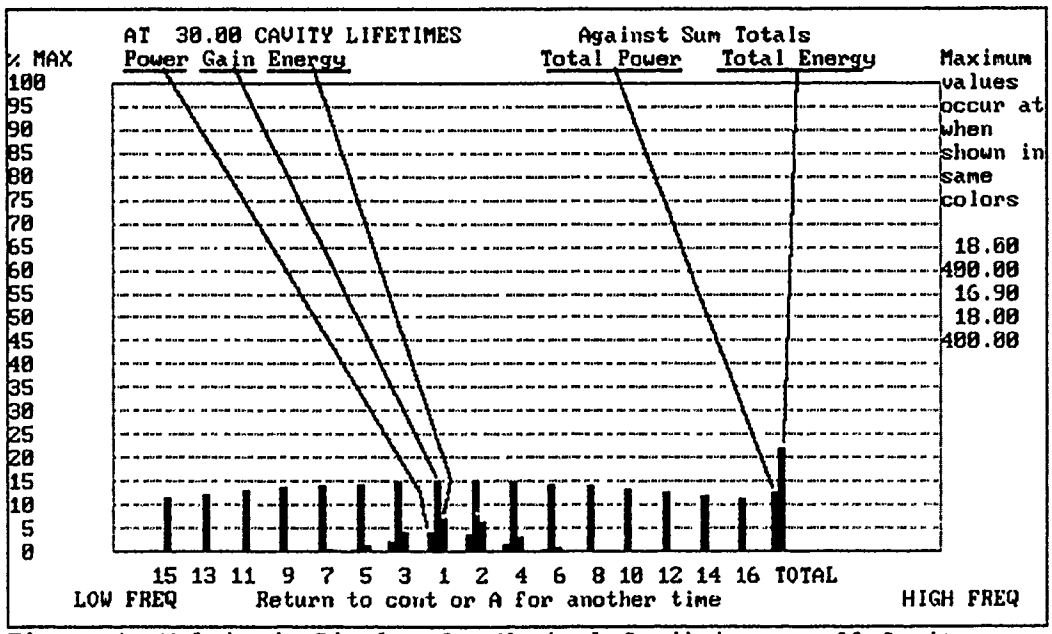

Figure 4 Multimode Display for Nominal Conditions at 30 Cavity Lifetimes

Figure 5 shows the same display at 400 cavity lifetimes. Figure 6 highlights the peak power distribution normalized to the total power at

the instant of peak power for the nominal case. Figure 7 shows the same distribution normalized to the largest peak power of all of the modes.

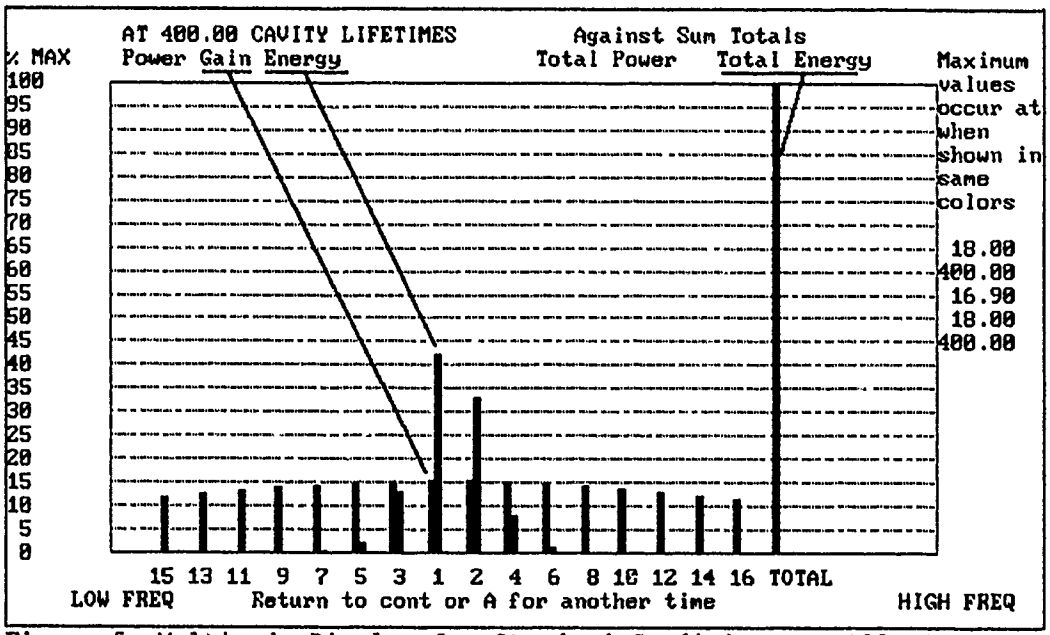

Figure 5 Multimode Display for Standard Conditions at 400 tCav

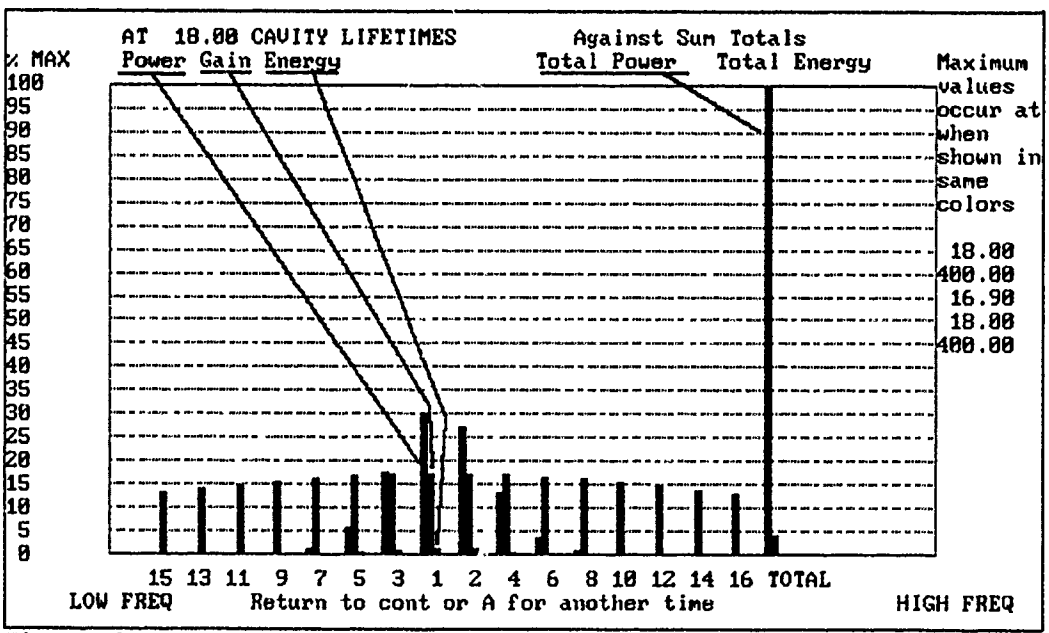

Figure 6 Display at 18 tCav Scaled against the Sum Total Peak Power

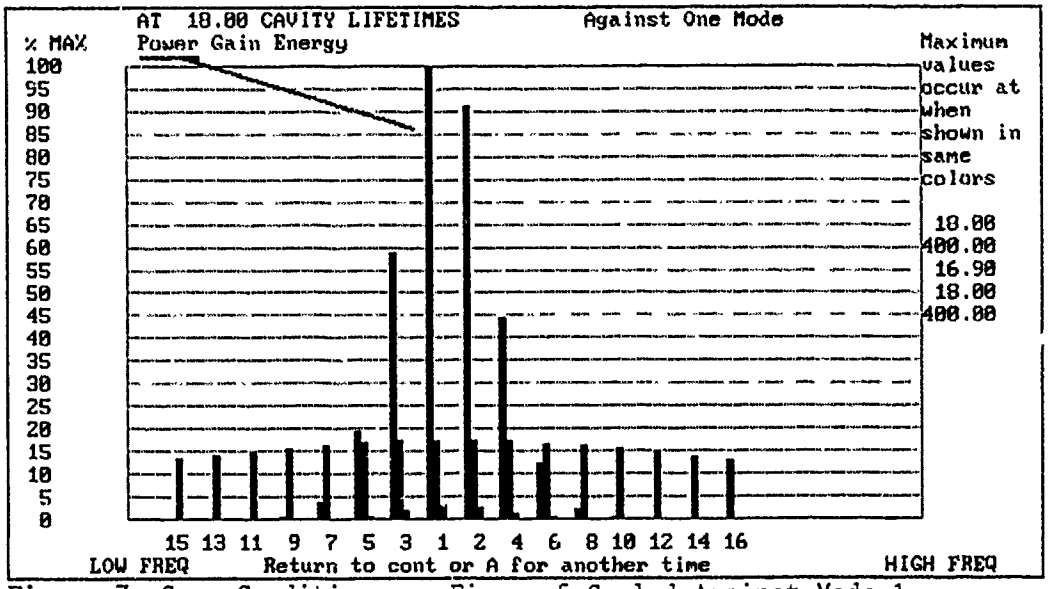

Figure 7 Same Conditions as Figure 5 Scaled Against Mode 1

The gain components on the multimode and time evolution displays are always scaled to the largest gain of any single mode as shown in Figure 8. The time evolution display will show a single mode's characteristics over the life of the pulse as seen for natural modes in Figure 9.

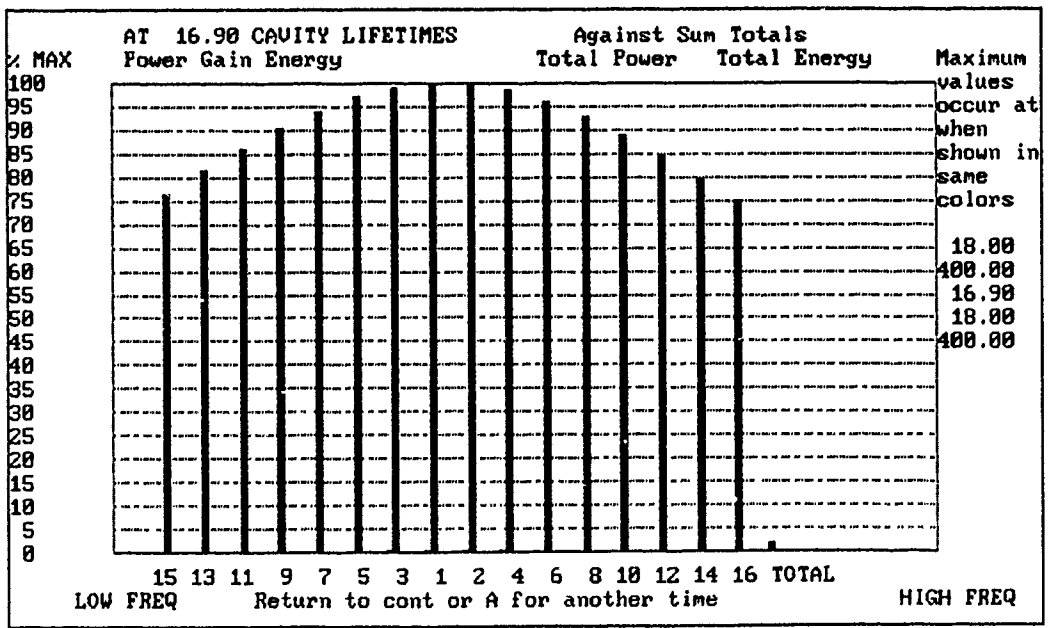

Figure 8 Multimode Display at Occurrence of Peak Gain

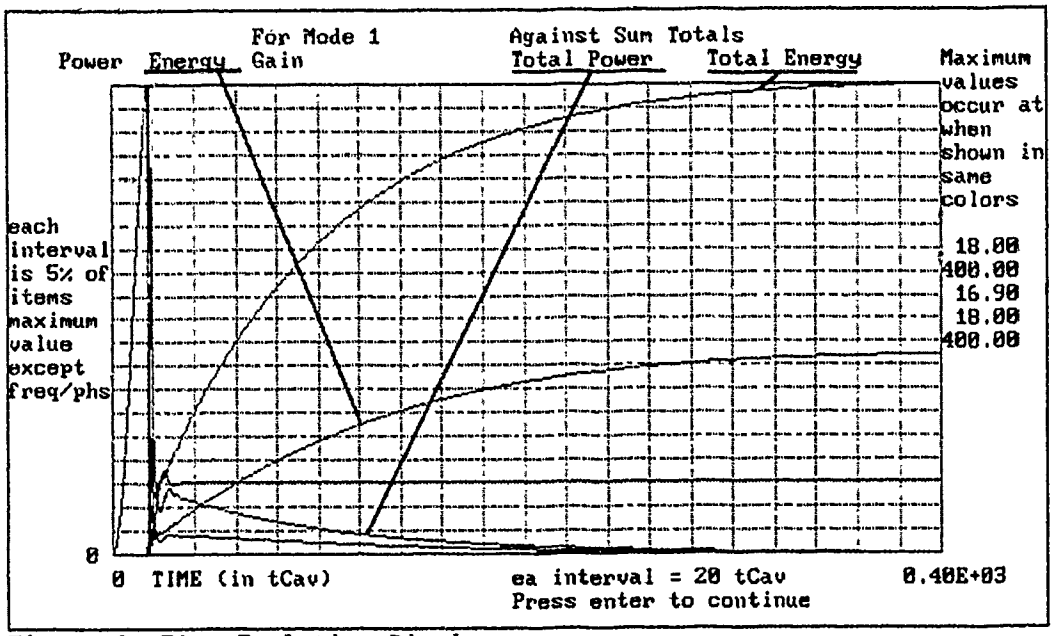

Figure 9 Time Evolution Display

Nominal Analysis for Step Size and Number of Modes

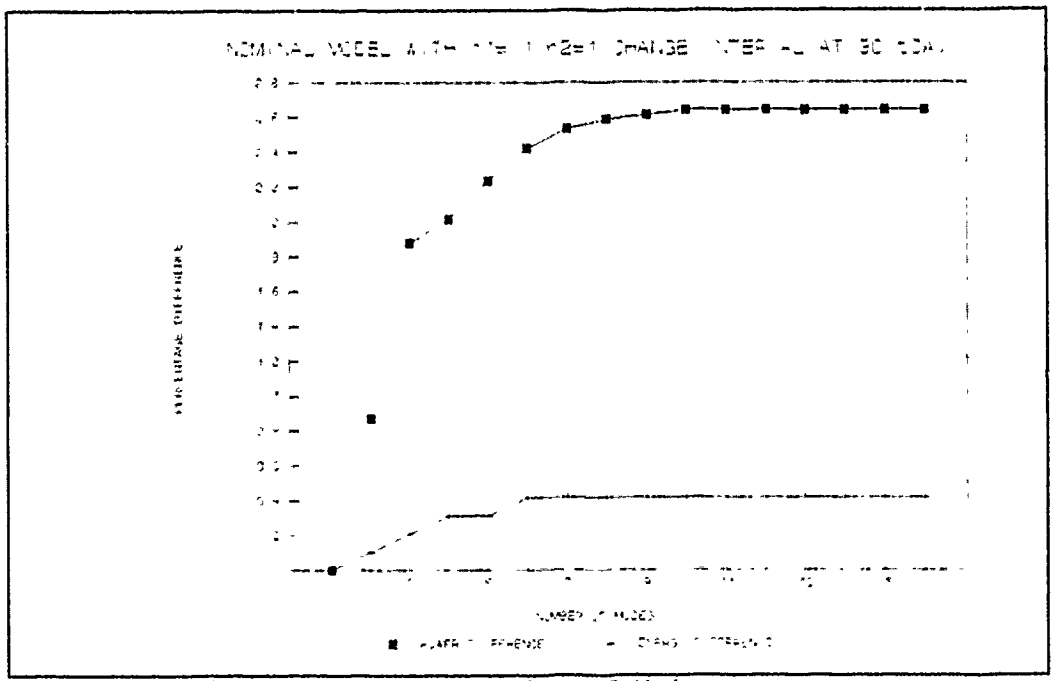

Figure 10 Nominal Analysis for Number of Modes

Two important decisions are the size of the interval and the number of modes to track. σ_e is inversely proportional to the amount of

frequency separation from the line center. As σ_e becomes smaller the critical inversion density increases. Thus, a mode with extreme spectral separation might have little effect on total power or energy. This details a dilemma: although more modes would better reflect the actual behavior of the laser, tracking additional modes requires more computing time and memory. Additionally, the length of time that the pulse evolution is tracked decreases. Coincidentally, the subinterval size used in the Runge-Kutta integration increases. Still another consideration is the fact that the entire populations N_a and N_b are available for all the modes. The center modes will depopulate the inversion quicker than any outlying modes. With the entire population inversion funneling through one mode the total power is larger than the summation of power for multiple modes. The number of modes that are required for the computations to be within 10% accuracy is the primary consideration. Figure 10 shows that any number of modes will match this requirement. The graph shows the percentage difference between the number of modes for total energy and peak total power against the condition of tracking one mode only. A better criteria is the comparison of the minimum number of modes required to closely match the maximum mode case. Figure 11 is a comparison of the summed peak powers and total energy for the 1, 3, and 16 mode case. The interval step size was chosen for the stable solutions under 0.2 cavity lifetimes plotted against the single mode case using a step size of 0.005 cavity lifetimes. Figure 11 shows a clear degradation for increasing time steps. The limitation for a consistent solution is 0.19 cavity lifetime for h1. For step sizes larger than 0.19 the results fluctuate from interval to interval. The solution for three modes with h1=0.19 is within 9.8% of the similar value for h1=0.005 and 16 modes. The limitation of this approach is the focus on the peak power. Any approach considering total energy alone results in a step size of almost

arbitrary size because the peak power pulse has little effect on the total energy, less still on the energy of any one mode.

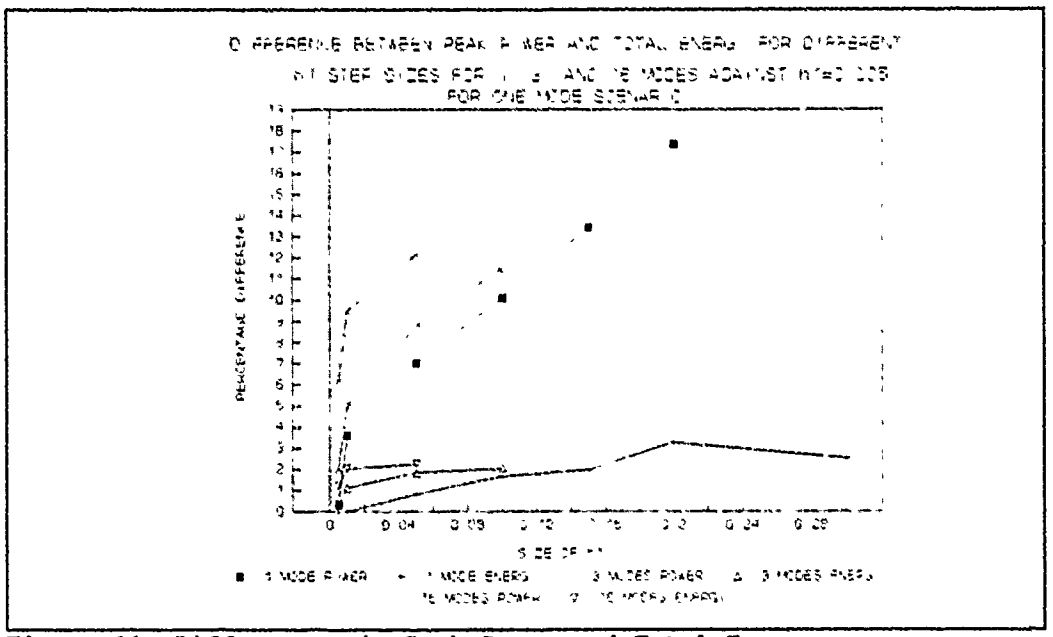

Figure 11 Differences in Peak Power and Total Energy

Nominal Analysis for Pressure and Step Size

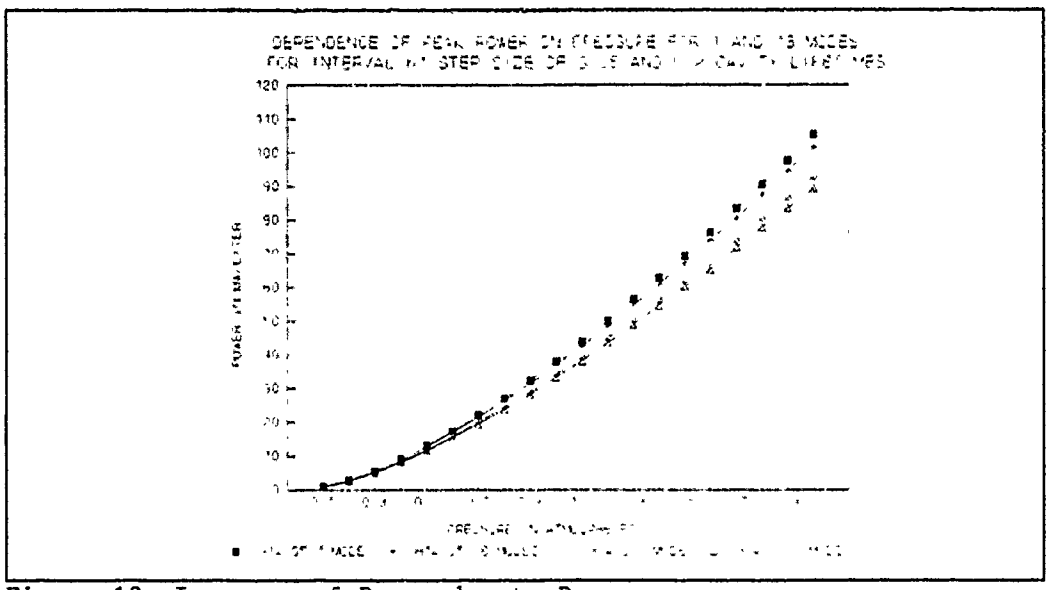

Figure 12 Increase of Power due to Pressure

Increasing the pressure of the system has two effects. First it increases the pressure broadened bandwidth. Secondly, pressure affects

the gain of the system and hence the power output in an almost linear fashion from 0.1 to 2 atmospheres as seen in Figure 12. Increasing the pressure also affects the allowable step size as seen in Figure 13. The relationship between pressure and interval size is not linear. The interval step size must decrease to accurately record the peak power as pressure increases. In Chapter VI the validation of this model is at 1 atmosphere. Accordingly the step size of h1=0.19 is within the desired 10% accuracy.

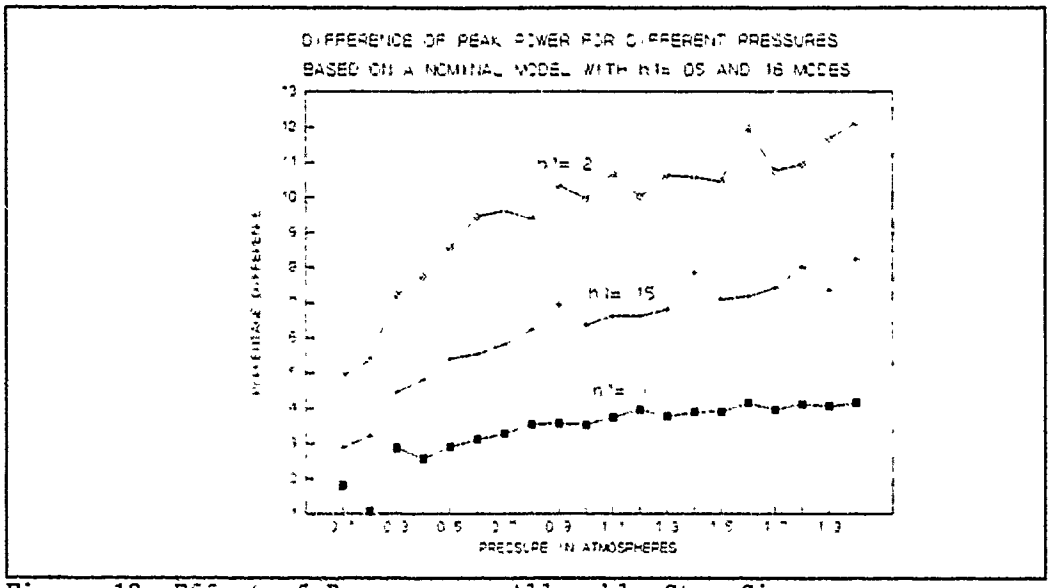

Figure 13 Effect of Pressure on Allowable Step Size

Increasing the number of modes weakens the assumption that the P(20) transition is isolated from the P(18) and P(22) transitions. The spectral separation between modes is 150 MHz with a cavity size of 1 meter. However, the separation between the P(20) and P(18) lines is 54283.22 MHz and the P(20) and P(22) lines are separated by 53548.92 MHz (13:24). This large separation precludes influence by populations in another transition for the maximum number of modes on each side of the transition frequency. Increasing the gain does effect the maximum allowable step size. Phenomenologically speaking the higher pressure causes higher gain which in turn increases the change in populations and

flux density during a set step size. As seen in Figures 10 and 11 the difference between 1 and 16 modes for peak power is well within 10% for step sizes up to h1=0.2 for any of the detailed pressures. The maximum allowable step size does vary with pressure as seen in Figure 13. Although h1=0.19 is a sufficient step size for pressure under 1.2 atmospheres a smaller step size is required at higher pressures. A single mode case study always has a larger power than a multimode case study. This is not due to the fact that in a multimode study some frequencies represent a larger potential energy in photon energy while others are smaller. At these frequencies and cavity sizes the difference is not that large - the difference between energy of a photon between adjacent modes is less than 0.001%. The mode associated with the largest σ_e will have the largest gain in the noninjected case. The discrepancy in gain leads to a larger flux density for the associated mode. The larger flux density stimulates a larger percentage use of the available population of the upper state. When the total upper state supports the mode with largest σ_e, the peak power increases. The change in flux density from Eq (2) is directly proportional to the size of the σ_e and the flux density. The spontaneous flux density is also proportional to the σ_e. The initial flux also has a direct effect of the charge in flux density. Clearly, the largest σ_e has an advantage in the nominal case. This is not true in the injected case. A large injected signal flux may influence the pulse evolution more than the σ_e. In a continuous, homogeneously-broadened laser, the gain is eventually reduced to threshold levels. The mode closest to line center has the highest gain. This mode also has the largest σ_e.

Chapter V Literature Review

In this chapter the significant literature is reviewed in chronological order. Lachambre used a modified flux-population rate equation with a conversion from field to flux. Siegman and Tratt et al both agree with Lachambre's approach and validate his findings of the injected mode selection range. Recently Cassard and Lourtioz used Maxwell's equations to predict conditions when two or more signals would exist simultaneously.

Lachambre's Approach

Lachambre developed the first locking study of TEA CO_2 using a combined population and field approach. He described the injected field in the manner of Chapter III. His results showed three major regions: a region where the injected signal had no effect; a region where mode selection existed for a wide variety of phases and powers; and a region where injection locking would occur with very small detuning angles and very large injected powers. Even for low powers an injection range of almost 0.4π in phase was observed. He based his efforts on a constant σ_e for the CO_2 molecule and for a total of 12 longitudinal modes. The results are instructive as depicted in Figures 14, 15, and 16. Figure 14 shows the relationship between the initial detuning angle or offset and the portion of the total pulse energy due to the injected signal. The vertical scale is the portion due to the injected signal E_i over the sum total of the injected signal plus the energy in the natural modes E_s. The injected signal has a strength of $5 \times 10^{(7-2m)}$ W/cm^2 where m is a number from 2 to 9 as detailed on the figure. The portion of the total energy due to the injected signal is very high for detuning angles under 36° for the injection powers shown. For any signal injected with an offset of 0.5π or greater there is little contribution from the evolving field to the total energy.

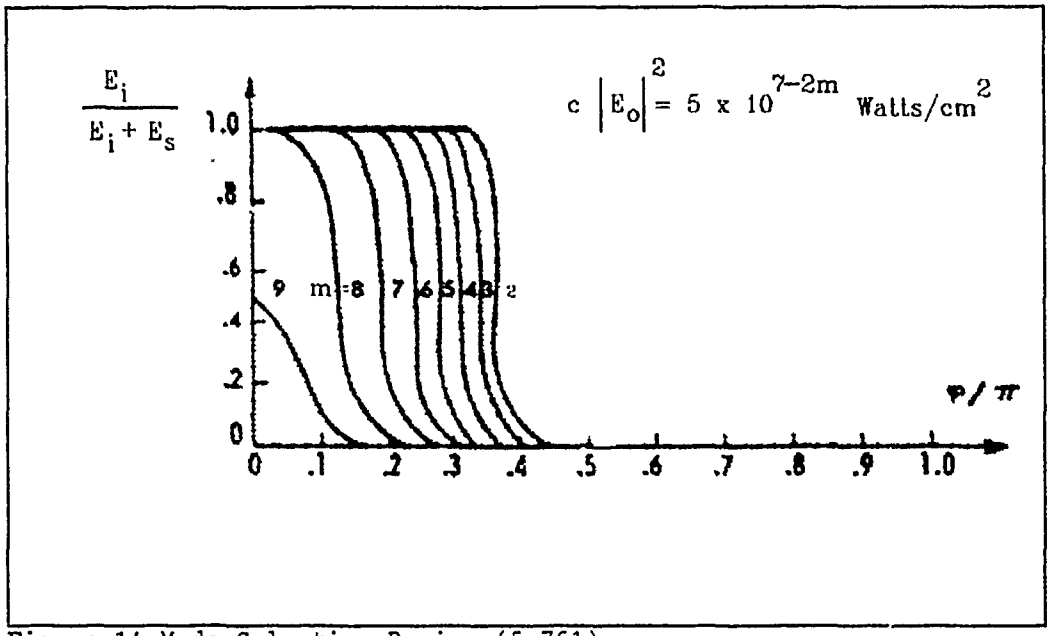

Figure 14 Mode Selection Region (5:761)

In Figure 15 the injected signal exhibits definite effects on the evolving signal. According to Lachambre the total peak power of all the natural modes when the detuning angle is 0.5π is 45 MW/liter with the peak occurring at 700 nanoseconds for a total energy of 4.4 Joules/liter (5:759). A strong injected signal causes an early reduction in the population inversion. This is seen in Figure 16 by the earlier peak power at 600 nanoseconds and the reduced peak power of 29 MW/liter. The total energy increases to 4.5 Joules/liter due to the longer power pulse. The lower charts in Figures 15 and 16 depict the value of $2\tau\dot{\theta}/\phi$ on the vertical axis where 2τ is the round trip time, θ is the instantaneous change in the phase and ϕ is the initial detuning angle of the injected signal form the nearest natural mode. If the quantity $2\tau\dot{\theta}$ is equal to ϕ then the evolving signal follows the detuning angle. This is termed the mode locked condition and the injected signal is said to operate in the mode selection region. If $2\tau\dot{\theta}$ is equal to zero the amplified injected signal is not locked to the detuning angle and is locked to the amplified injected signal. This is the true injection

locked case. In the low power case we see a beat frequency oscillation in Figure 15. This is due to the competition between the mode and the injected signal when the selected mode's power decays. High power

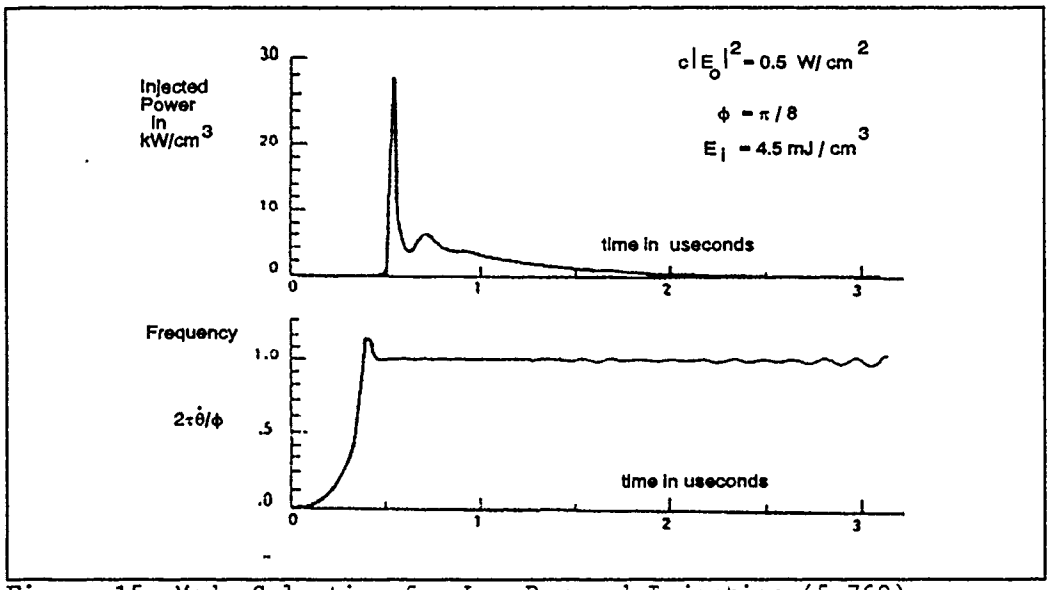

Figure 15 Mode Selection for Low Powered Injection (5:760)

injection causes an earlier reduction in the inversion before locking to lock to the injected signal. This suggests that injection locking is

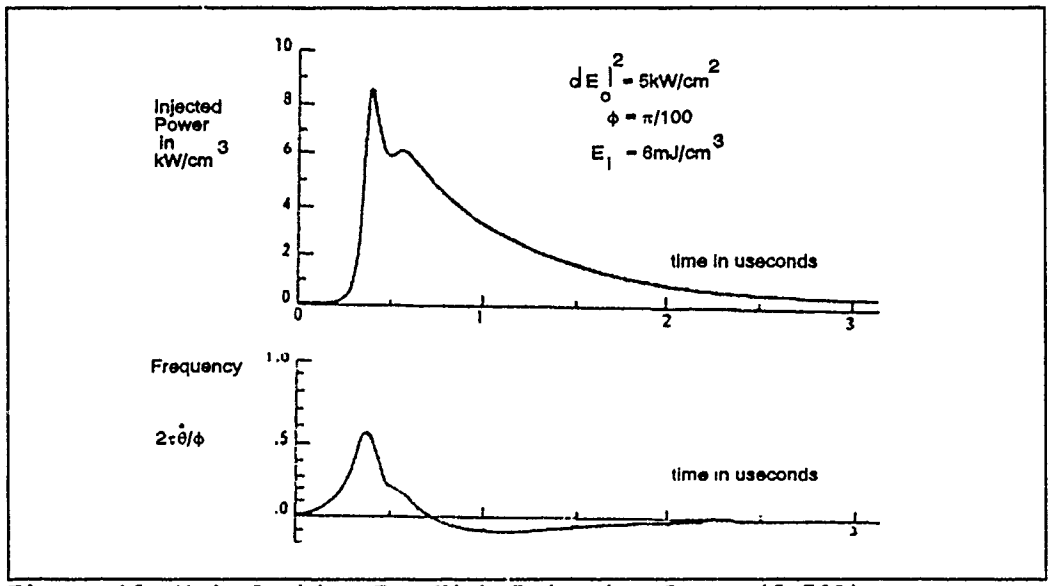

Figure 16 Mode Locking For High Injection Power (5:760)

possible only when the gain is low (below threshold). Figure 16 shows the signal evolution at very small detuning angles with very high injected powers. The injected power peak is reduced even further to 9 MW/liter. The peak power occurs even earlier at 500 nanoseconds. The secondary peaks are less extreme and the pulse tail is longer. The signal is effectively injection locked, and the total energy in the injected signal increases to 6 Joules/Liter.

Tratt CO_2 Laser Injection Study

Tratt completed an extensive review of injection seeding in 1985. This effort detailed the active mode selection schemes which lead to the selection of one single longitudinal mode (SLM) (Tratt:235). The features of these schemes show a suppression of the gain switched spike of radiated power and a longer tail over the time of the pulse as depicted in Figure 17 (11:237).

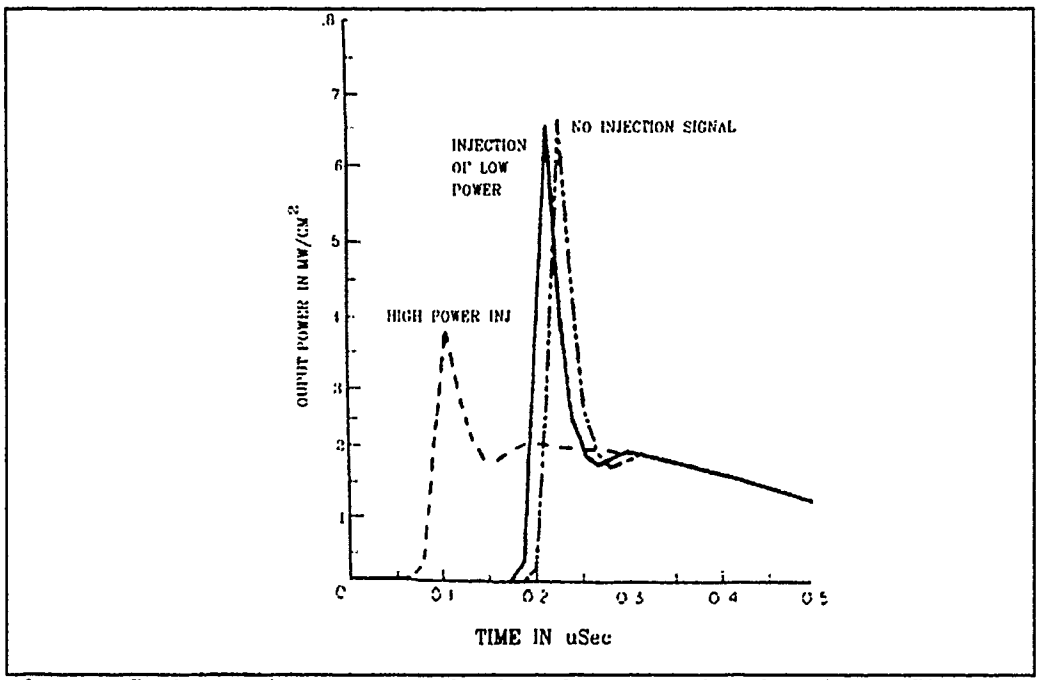

Figure 17 Change in Power Evolution due to Injection (11:237)

As seen in Figure 17 the introduction of a signal causes early depletion of the inversion level and leads to earlier signals and lower

powers. Eq (48) is the w··e used in his analysis and is similar to the description in Chapter II.

$$\vec{E}(t) = \sqrt{R}\,\vec{E}(t-2\tau)e^{[G(t)+j\phi]} + \vec{E}_{injected} \tag{48}$$

Here G(t) is the real part of m(t) expressed in Eq (16) of Chapter II, R is the reflectivity of the secondary mirror and ϕ is the imaginary part of m(t) from Eqs (12) and (16) earlier. The steady state solution (11:245) of Eq (48) is when G(t)=0. Eq (48) is separated into real and imaginary parts. This results in the real part of the field, $\Re$, and the imaginary part, $\Im$, as:

$$\Re\,[E(0)] = E_{injected}\,\frac{1-\sqrt{R}\cos\phi}{1+R-2\sqrt{R}\cos\phi} \tag{49}$$

$$\Im\,[E(0)] = E_{injected}\,\frac{\sqrt{R}\sin\phi}{1+R-2\sqrt{R}\cos\phi} \tag{50}$$

From these two expressions Tratt developed an expression for the round trip phase shift $\theta(t)$ as:

$$\tan[\theta(t)-\theta(t-\tau)] = \frac{\Im[E(t)]\,\Re[E(t-\tau)] - \Re[E(t)]\,\Im[E(t-\tau)]}{\Re[E(t)]\,\Re[E(t-\tau)] + \Im[E(t)]\,\Im[E(t-\tau)]} \tag{51}$$

and the instantaneous frequency F(t) becomes $(\theta(t)-\theta(t-\tau))/\phi$ (11:245). The implications are that a zero phase shift indicates a locking to the injected signal but that a phase shift change implied a resonance condition with the nearest cavity mode like Lachambre. Tratt documented the three regimes noticed by Lachambre (11:246). Tratt noticed the existence of the beat frequency oscillations in the higher power cases due to interactions between the existing cavity signal and the injected signal (11:246-247).

Tratt found that injected signals with a detuning angle from zero to π had an effect on the power output profile. The effects became less noticeable for larger and larger offsets as depicted in Figure 18. Many authors agree with the limitation of the detuning angle of 0.4π for

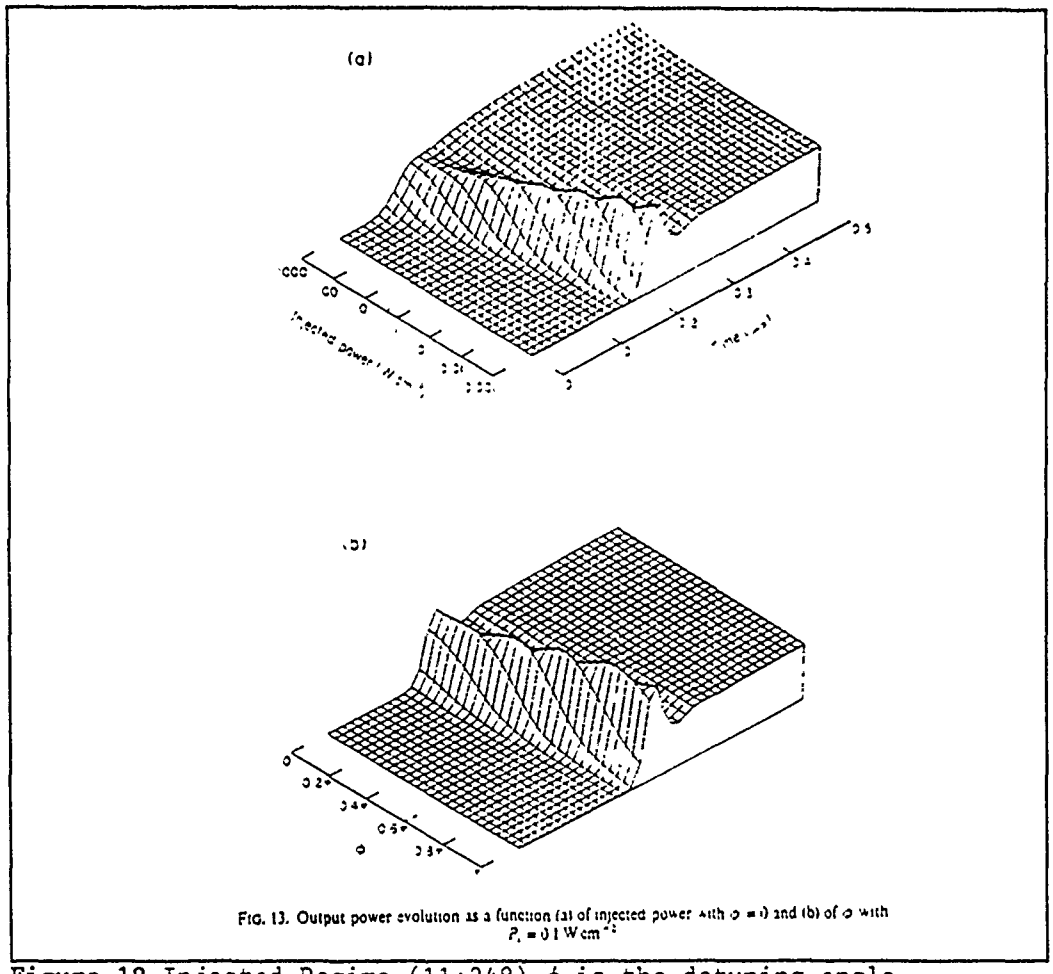

FIG. 13. Output power evolution as a function (a) of injected power with $\phi = 0$ and (b) of ϕ with $P_i = 0.1\ W\,cm^{-2}$

Figure 18 Injected Regime (11:248) ϕ is the detuning angle

injection locking. However, other authors using large cavities found that injection locking could be forced over the entire spectrum (11:260).

Siegman's Derivation

Siegman objects to the practice of using the term "injection locking" because the injected signal provides a set of initial conditions from which the wave grows with little regard to the injected signal. He would rather the term "injection seeding" apply in this scenario. In a laser cavity the wave circulating at a time t, $E_{circ}(t)$, would be the sum of the previous circulating wave that is just reflected

off the mirror, $E_i(t)$, and the injected wave, $E_o(t)$, using the expressions below (8:1155):

$$\vec{E}_{circ}(t)=\vec{E}_i(t)+\vec{E}_o(t) \tag{52}$$

$$\vec{E}_i(t)=\vec{E}_{circ}(t-2\tau)\,e^{[g-j2\tau(\omega_{inj}-\omega_{osc})]} \tag{53}$$

where g refers to the cumulative gains inside the cavity of the previous wave at time $t-2\tau$, ω_{osc} is the frequency of the nearest longitudinal mode, and ω_{inj} is the frequency of the injected signal. When the cavity is below threshold and the signals are on resonance the vectorially added signal results in a steady state nominal wave. The injected signal makes up the vectorial difference between the circulating wave and the longitudinal mode. For injected signals of low power there are distinct possibilities for injection seeding. After separating the variables and using Euler's identities for exponents (8:1156):

$$\vec{E}_{circ} = \frac{1}{\left[1-e^{-g}\cos\left(2\tau\,(\omega_{inj}-\omega_{osc})\right)\right]+j\left[e^{-g}\sin\left(2\tau\,(\omega_{inj}-\omega_{csc})\right)\right]}\vec{E}_i \tag{54}$$

This expression shows that for the signal to build the subexpression $|2\tau(\omega_{inj}-\omega_{osc})|$ must be less than $\pi/2$. When the instantaneous phase $\phi(t)$ is designated as Siegman did (8:1160):

$$\begin{aligned}\phi(t) &\approx -(\omega_{inj}-\omega_{osc})\,T\cdot\frac{t}{T}\\ &\approx -(\omega_{inj}-\omega_{osc})\,t\end{aligned} \tag{55}$$

then the actual frequency $\omega_i(t)$ is simply:

$$\begin{aligned}\omega_i(t) &= \frac{d\phi(t)}{dt}+\omega_{inj}\\ &\approx -\omega_{inj}+\omega_{osc}+\omega_{inj}\\ &\approx \omega_{osc}\end{aligned} \tag{56}$$

From Eq (55) and using a expansion of the equation in the form of

$$f(x+h) = f(x) + hf'(x) + \frac{h^2}{2!}f''(x)\ \langle etc\rangle \tag{57}$$

based on the assumption that $\omega_i-\omega_o \ll 1/(2\tau)$ Eq (52) becomes:

$$\frac{d\vec{E}_{circ}}{dt} + \left[\frac{g}{2\tau} + j(\omega_{inj}-\omega_{osc})\right]\vec{E}_{circ} = \frac{1}{2\tau}\vec{E}_o \qquad (58)$$

The implication from Eq (56) is that the frequency of a mode selected laser is almost entirely on the resonant mode wavelength and for all practical purposes the injected contribution is buried. This is phenomenologically correct when the circulating wave is much bigger than the injected signal in a mode selected regime.

Cassard and Lourtioz Approach

Cassard and Lourtioz approached the process from Maxwell's equations and assumed linearity. A wave equation of motion for the complex field $\vec{E}$ in a medium with a polarization $\vec{P}$ and current density $\vec{J}$ is:

$$\Delta_r E - 2jk\left(\frac{dE}{dt} + \frac{dE}{c\,dt} + \frac{\sigma}{2\epsilon_o c}E\right) = -\mu_o\omega^2 P \qquad (59)$$

where σ is the conductivity and ω is any arbitrary mode frequency (2:2322). After fixing the boundary conditions they developed a set of eigenmodes (2:2322). Their solution provides for the injected field (2:2324) as Eq (60):

$$E(t+2\tau) = \left(E(t) + \frac{E_{inj}}{\sqrt{R}}\right)\sqrt{R}\, e^{\int_t^{t+2\tau} cg(\theta)\,d\theta}\, e^{-2j\pi\delta} \qquad (60)$$

where $g(\theta)$ is the complex gain term that includes resonant dispersion and $\delta = \tau/\pi(\omega_{inj}-\omega_c)$ and is equivalent to Lachambre's expression $cd\theta/2L$. In this instance the injected signal is measured prior to entering the cavity.

Cassard and Lourtioz objected (2:2321) to the assumption that Lachambre made concerning the lack of amplification of the injected signal. However, the injected signal would only experience amplification on one trip through the cavity. At the end of that trip, the injected signal is added to the circulating wave. Since the

circulating wave becomes much larger over time than a low power injection signal one can discount the contribution of the injected signal over time. This validates Lachambre's approach. For a high power injection signal there could exist an injected signal amplified by one trip through the cavity that adds vectorially with the evolving field. This would cause the evolving field to shift not only due to the offtuning of the cavity but also due to vector addition with the injected signal. There could exist more than one mode in the cavity but this regime will be confined to large injection powers.

Conclusion

The combination flux-population rate equation approach is valid for low power injection signals. The incorporation of line shape in the expression for cross section will yield more accurate results than Lachambre for there will be a dependence on mode selection and spectral separation for outlying modes. Three modes is enough to consider at atmospheric pressures - from the line shape factor the relative size of the mode at 8 free spectral ranges for the nominal mix is still 70% of the highest value but has little contribution to the total signal.

Chapter IV Results

This chapter discusses the results of the computer runs. The validation of the basic model is reviewed and the differences between Lachambre's results and the computer program are explained. The dependence of the evolving field on various physical parameters is depicted.

Validation

The simulation was run against the original model developed by Stone from Gilbert's article on CO_2 Lasers. There was no difference between the two simulations. Next the model was run in comparison to Lachambre's results. The program correctly predicted the same results for the peak power of 45 MW/liter but had a much earlier peak. There are two reasons for this discrepancy. The first is that Lachambre included in his population equations a collision transition between the 10°0 and the 02°0 as a relaxation process for the lower state. This rate was dependent only on CO_2, N_2, and He gas mixtures. He implicitly assumed that the relaxation from this state was very fast and that the possibility of the reverse transition was not likely. Although a relaxation operation is required from the 10°0 state to keep a strong inversion the method of using a lumped relaxation process is more accurate. The second difference is in the generation of spontaneous flux. In Chapter II the derivation of the spontaneous term was based on the population of the upper state and the fraction of the spontaneous emitted photons that intersect the secondary mirror. Lachambre used a different approach incorporating the concept of amplified spontaneous emission (ASE) and determined a one-way photon noise density to use as his field for the natural longitudinal modes (5:757). This results in a spontaneous flux density does not depend on the population inversion. The value for current default parameters is 10^9 times larger than

Lachambre. Accordingly our peak is much sooner. Since the flux builds rapidly once established, there is no effect on the peak power magnitude.

Additionally, Lachambre did not include the effects of a reduced active element size in his flux rate Eq (5:758). He accounted for a gain section length inside a larger resonator cavity only in his generation of ASE. He did not account for the possibility of the smaller section length in his field equations. The rate of change of the populations is not dependent on the power, but the density of the flux in the gain section affects the change in the upper and lower CO_2 states. This effect is significant. In the manner of Milonni (6:296) one must add the effect of the reduced active section length in the cavity to both the flux equation for the natural modes and the coupled equations for the injected field. Figure 19 shows how the peak output power is reduced as the length of the cavity increases with a constant gain section length.

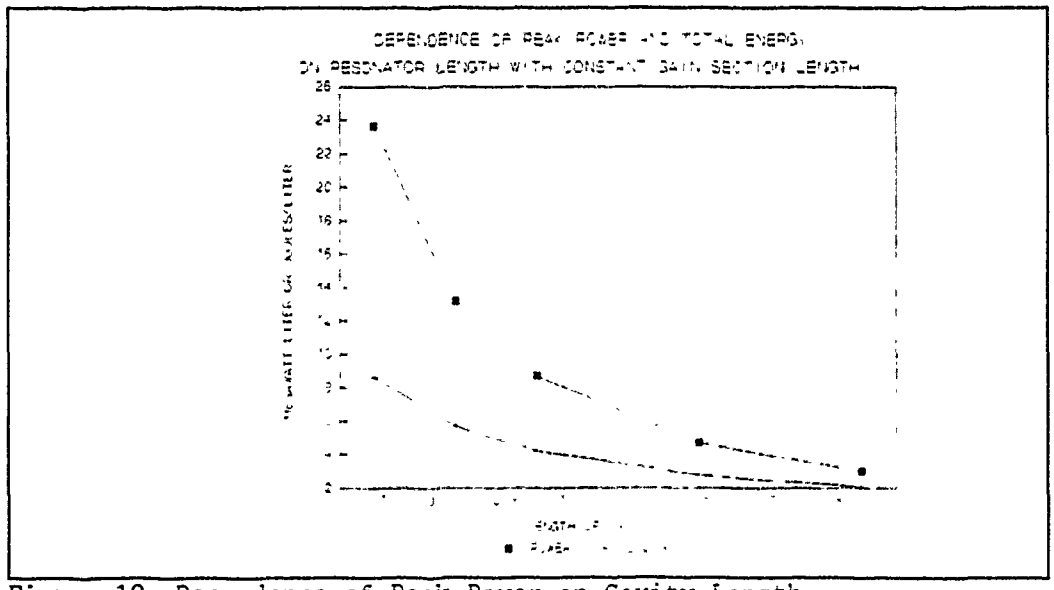

Figure 19 Dependence of Peak Power on Cavity Length

Figure 19 is a compilation for the default parameters with an active section length of 0.5 meters and a reflectivity of 90%. The pump

length and the integration step size were both adjusted for all events so that the pump duration was 300 nanoseconds and the integration step size was a constant 3.17 nanoseconds regardless of the cavity length.

In an continuous wave, non-injected scenario, the long term laser frequency belongs to that of the strongest mode. In a continuous wave laser under homogenous conditions similar to the present case, the modes with a smaller effective radiative cross sectional area are eventually quenched either by losses or filters and only the strongest signal survives. This is somewhat true in this study as well. Five modes are more than adequate to describe the power evolution as seen in Figures 4 through 7. In Figure 5 less than 3% of the total energy comes from Mode 5. From a phenomenological view one might think that smaller effective radiative cross sectional area would effect the mode selection range. While this is true with small pressure broadened bandwidths this is not the case at atmospheric pressures. Figure 20 depicts the relationship between injection near the strongest longitudinal mode and the next strongest mode for the default parameters.

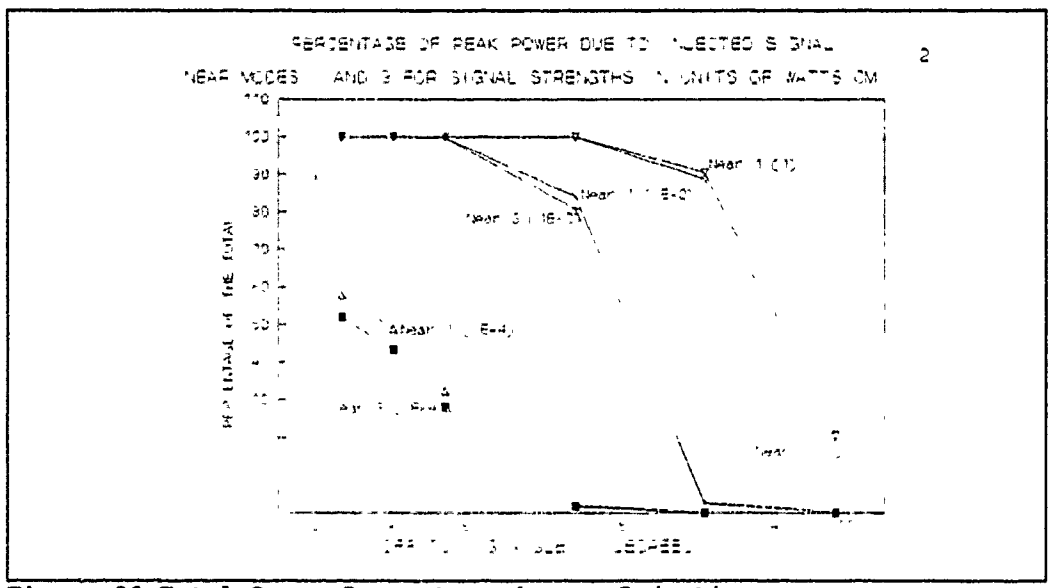

Figure 20 Total Power Percentage due to Injection.

There is not a significant relationship between the total energy of the injected signal for either mode one or mode three at atmospheric pressure. This effect is the same regardless whether injection is higher or lower in frequency around the chosen mode as long as the detuning angle is equal. Figure 20 also shows power and offset dependence similar to Lachambre's results.

The same effects that Lachambre noticed for injected signals are also apparent. There is a distinctive beat frequency oscillation as the total power weakens. This effect is more noticeable for higher injected powers and is still more noticeable as the total power weakens. As seen in Figure 21, the effect of the oscillation is low at the beginning. This oscillation does not occur during the peak power spike but at some later time. The oscillations become larger and larger. Lachambre noticed this as well (Figure 15).

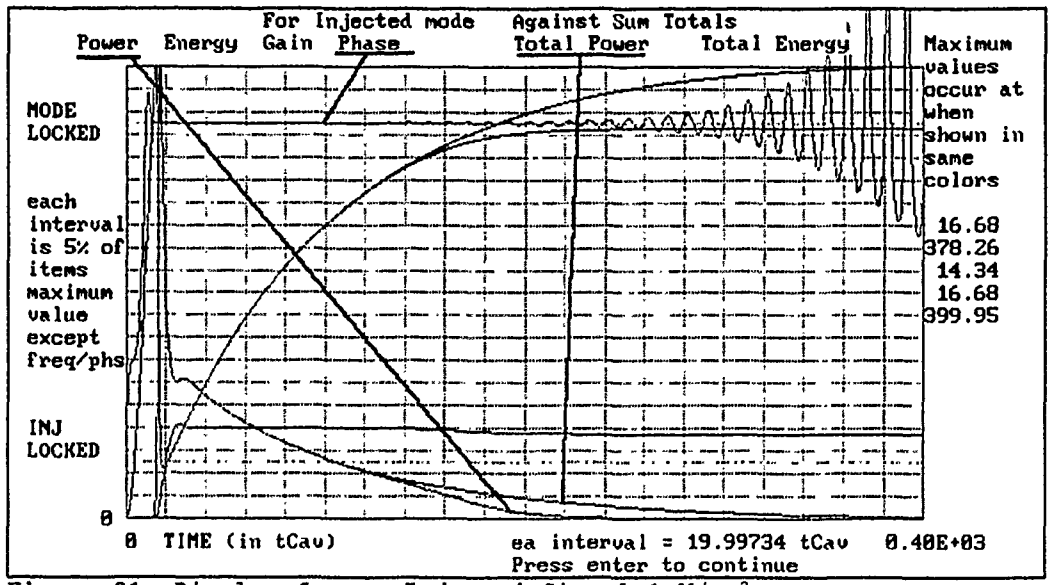

Figure 21 Display for an Injected Signal 1 W/cm^2

Figures 22 and 23 show how the phase oscillations increase in amplitude over time as the injected signal becomes larger. Figure 22 shows that as the injected signal is increased the phase oscillation becomes progressively larger. Later in the pulse, the effect of the

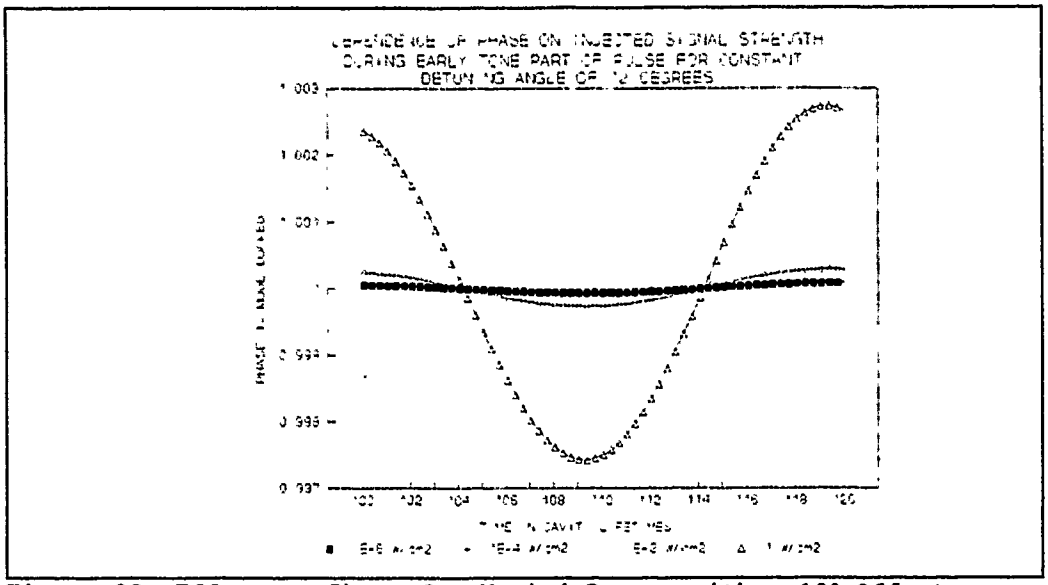

Figure 22 Effect on Phase for Varied Powers with a 12° Offset

oscillation is more noticeable as shown in Figure 23 for the same conditions for Figure 22. If the time is continued out much longer, as in Figure 24, the oscillation gets larger and larger then abruptly becomes injection locked; however, the output signal is so weak that the signal serves little value.

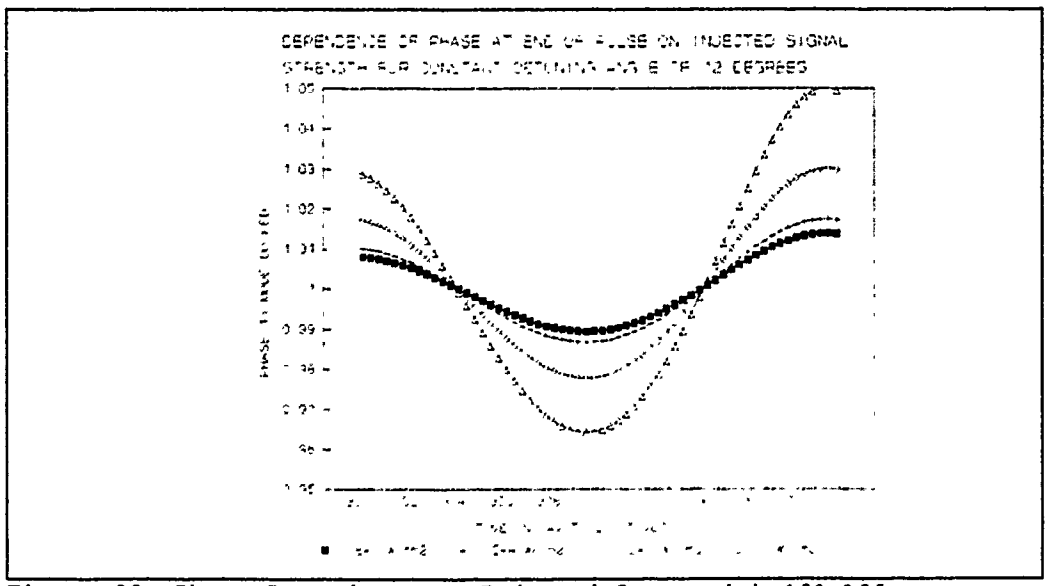

Figure 23 Phase Dependence on Injected Power with 12° Offset

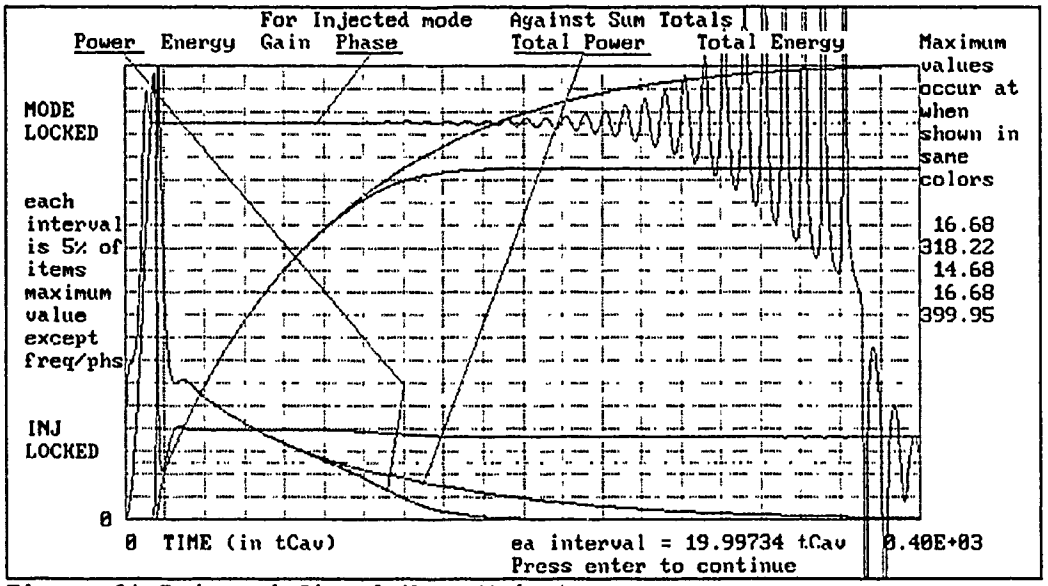

Figure 24 Injected Signal Near Mode 4

Another noticeable characteristic is that the phase closely follows the rising gain curve as seen in Figure 25. Figure 25 shows the evolution of an injected signal near Mode 4 at a detuning angle of 24 degrees with an injected power of 1 Watt/cm^2. The most influencing factor in Eq (43) is the factor η. η is the ratio of the evolving field

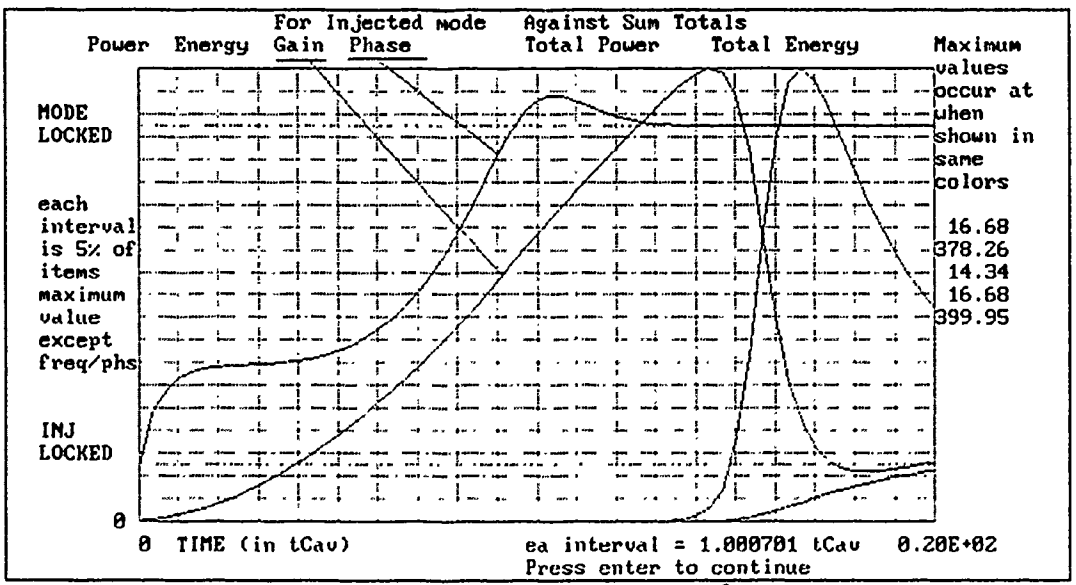

Figure 25 Display for Injected Signal of 1 W/cm^2 (Mid Pulse)

over the injected field. As the evolving field becomes larger, the second term in the differential phase Eq (37) becomes smaller. This results in a dependence on the initial offtuning angle exclusively.

Figures 26 through 29 show the lack of dependence of the amplified injected signal on the mode number nearest the injected signal.

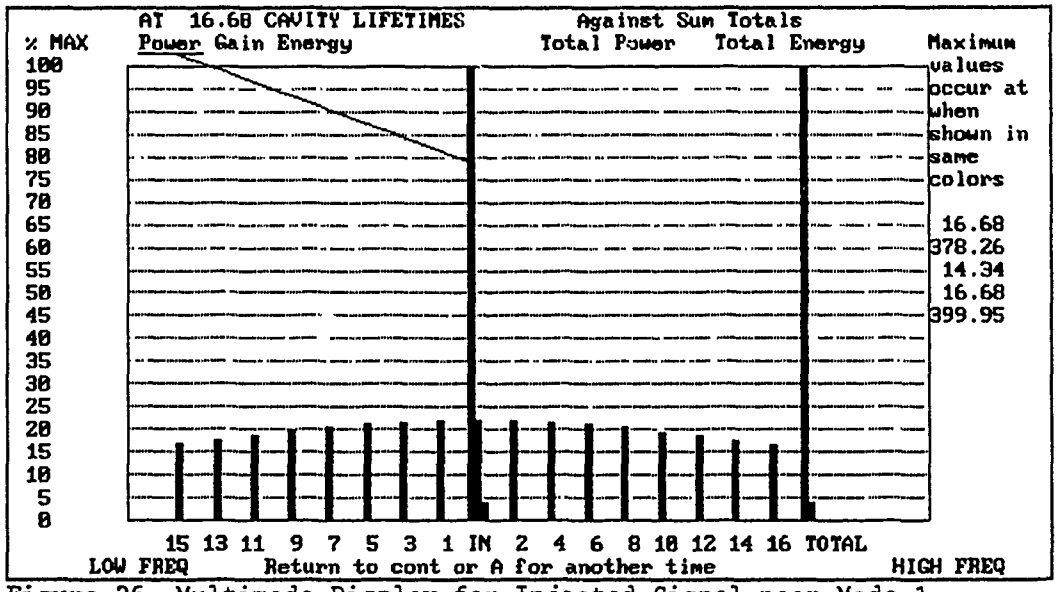

Figure 26 Multimode Display for Injected Signal near Mode 1.

Figure 26 is based on injection near Mode 1 using the standard conditions with a detuning angle of 24 degrees and an injected signal of 1 Watt/cm^2. The injected signal peak power clearly dominates all longitudinal modes. Figure 27 is based on injection near mode 4 using the same conditions as Figure 26. The dominance of the injected signal is clear in Figure 27 as well. In a mode selection regime all of the peak power is due to the injected signal as exemplified in Figures 26 and 27.

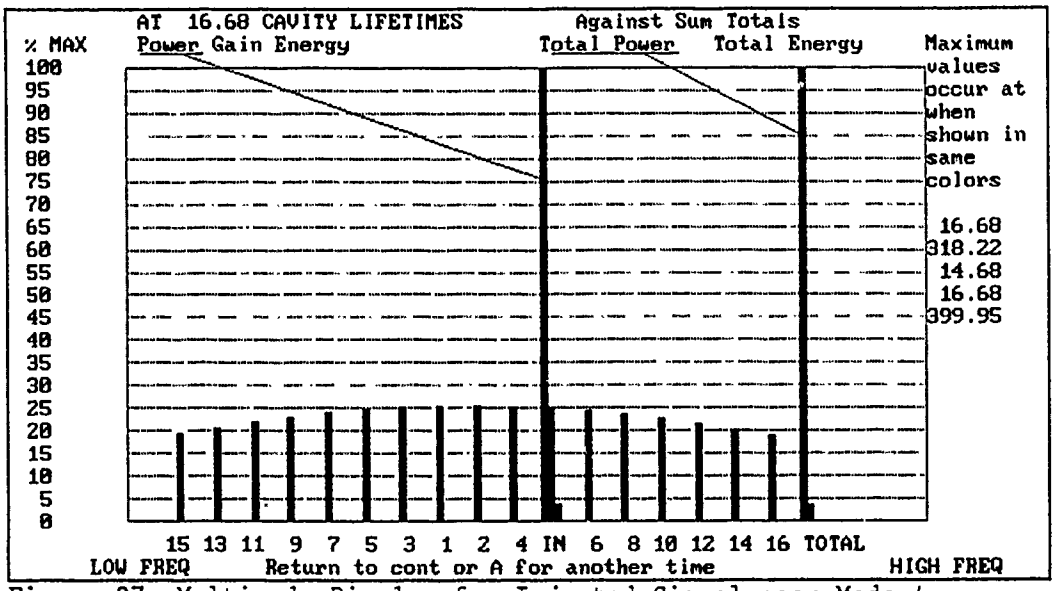

Figure 27 Multimode Display for Injected Signal near Mode 4.

However, due to the larger spontaneous generation of flux by natural longitudinal modes incorporated in this work the total energy contribution by the injected signal is not as dominating. This is shown in Figures 28 and 29.

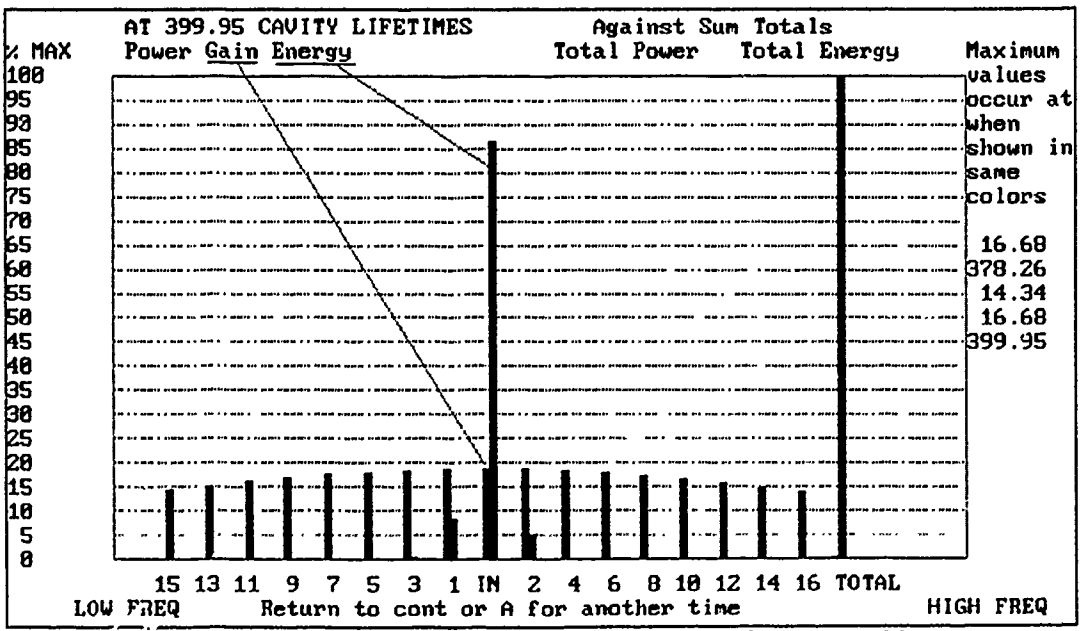

Figure 28 Display of an Injected Signal near Mode 1 at 400 t_{CAV}.

For an injected signal near Mode 1 the contribution by the injected signal is 86% of the total for the given conditions.

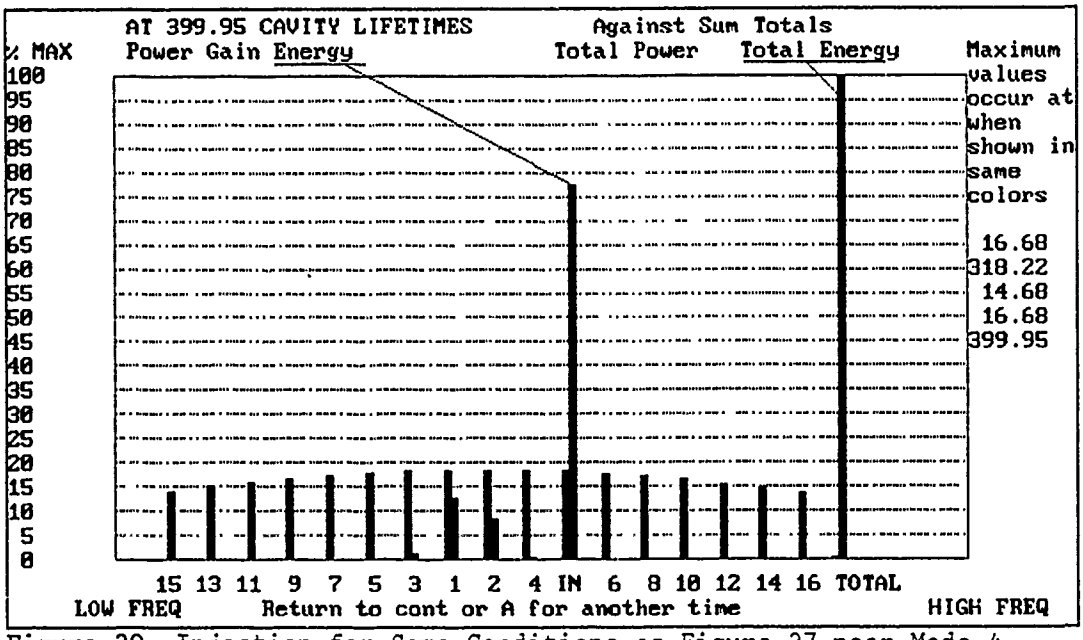

Figure 29 Injection for Same Conditions as Figure 27 near Mode 4

For an injected signal near Mode 4 the same injected signal strength is only 77% of the total. The injected signal suffers from inconsistent boundary conditions. A larger gain potential is required for the amplified injected signal than the natural longitudinal modes. As the gain decreases the amplified injected signal dies away. The remaining population supports the natural longitudinal modes. This difference in energy is reflected in Figure 24. Figures 28 and 29 use the same conditions as Figures 26 and 27.

Mode number has little effect on the injection locking regime as seen in Figures 30 and 31. In Figures 30 and 31 we used the default parameters with an injected signal strength of 5 KWatts/cm^2 at a detuning angle of 24 degrees. Figure 30 is for injection near Mode 1.

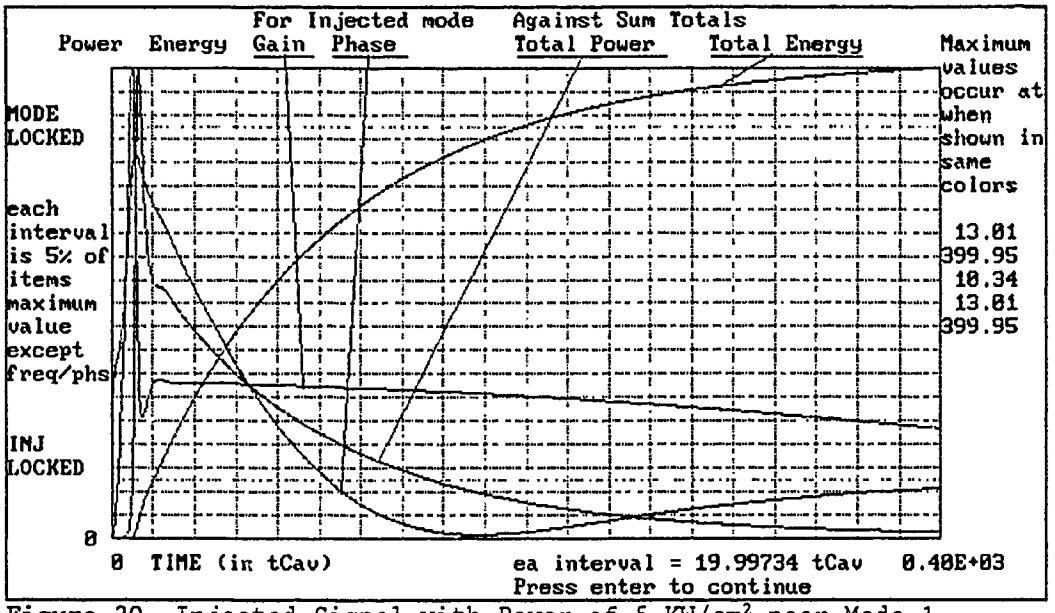

Figure 30 Injected Signal with Power of 5 KW/cm^2 near Mode 1

Figure 31 is for injection near Mode 4. In both cases the peak power is at the same time. The injection phase is also the same.

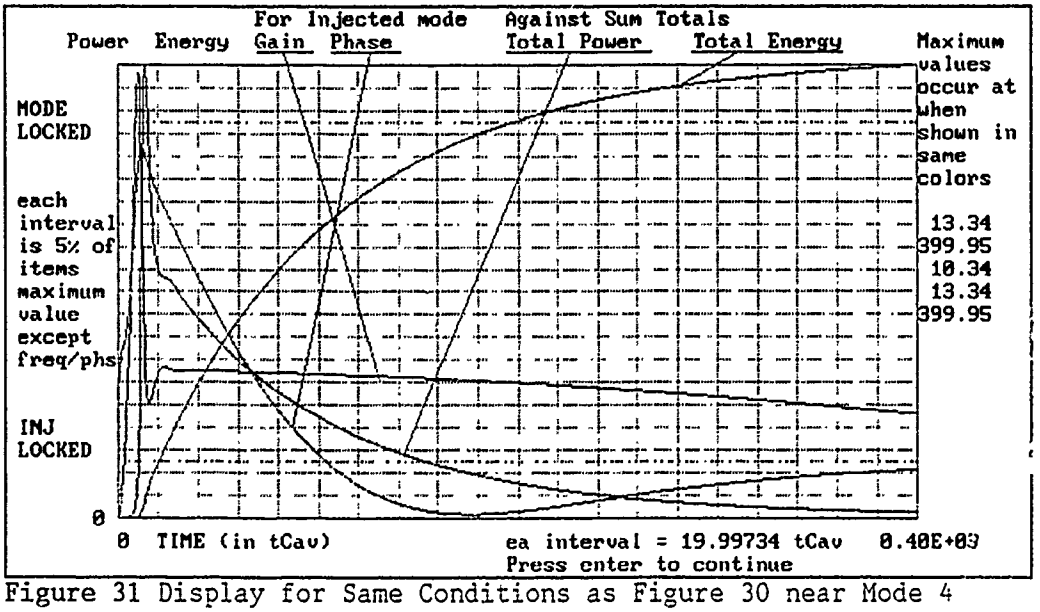

Figure 31 Display for Same Conditions as Figure 30 near Mode 4

Effect of Injected Signal Power on Power Evolution

An increased injected signal strength causes an earlier depletion of the population inversion. Consequently, as the injected signal

strength increases the peak power will decrease and the time of the peak is earlier. This is seen in Figures 32 through 34. Figure 32 shows the power due to the amplified injected signal for various strengths in the injection mode selection zone near mode one using the standard conditions.

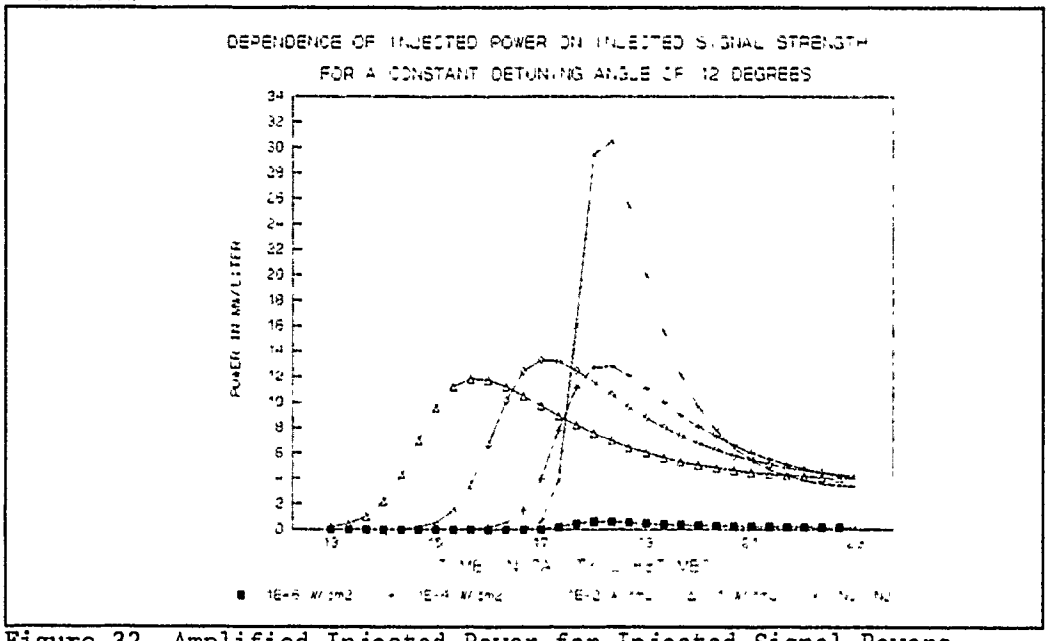

Figure 32 Amplified Injected Power for Injected Signal Powers

Figure 33 depicts the total power of all modes, whether spontaneously generated or due to the injected signal for a similar interval as shown in Figure 32. Notable is the effect on the total power due to a small injected signal. For an injected signal of 10^{-6} W/cm^2 the detuning angle is too large to allow mode selection. However, for a signal of 10^{-4} W/cm^2 the total power is 16 MW/liter (Figure 33) while the power due to the injected signal is 12 MW/liter. At the higher injection levels the power is due almost entirely to the injected signal with little contribution from the other modes.

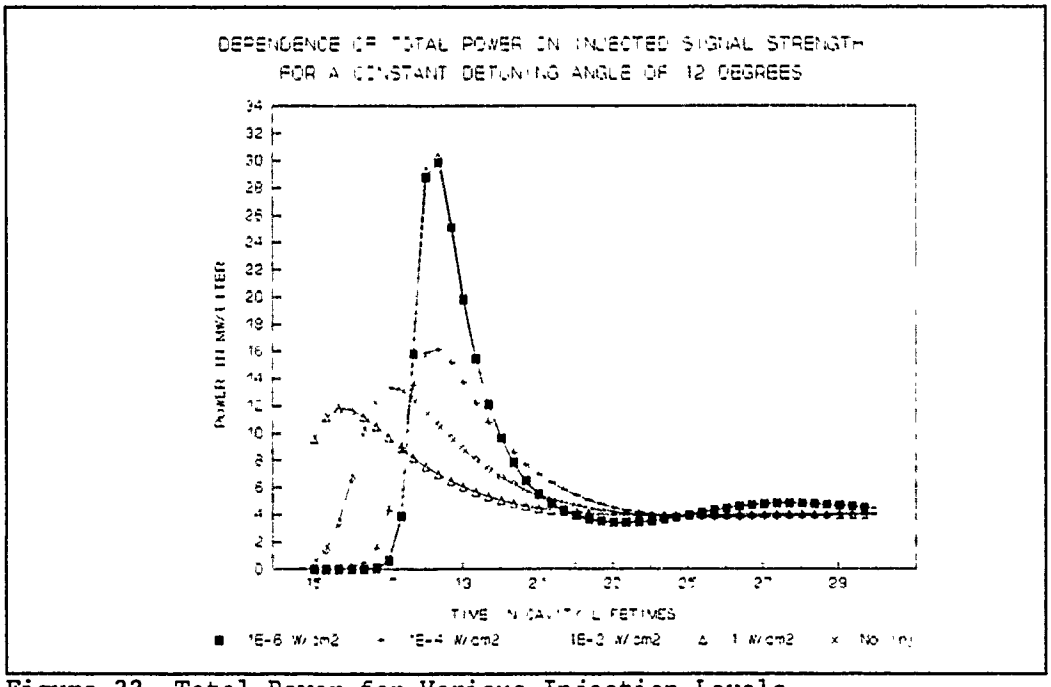

Figure 33 Total Power for Various Injection Levels

Figure 34 is a close up of mid-pulse power evolution to show how the higher signal levels deplete the population inversion faster and cause the power to dissipate faster.

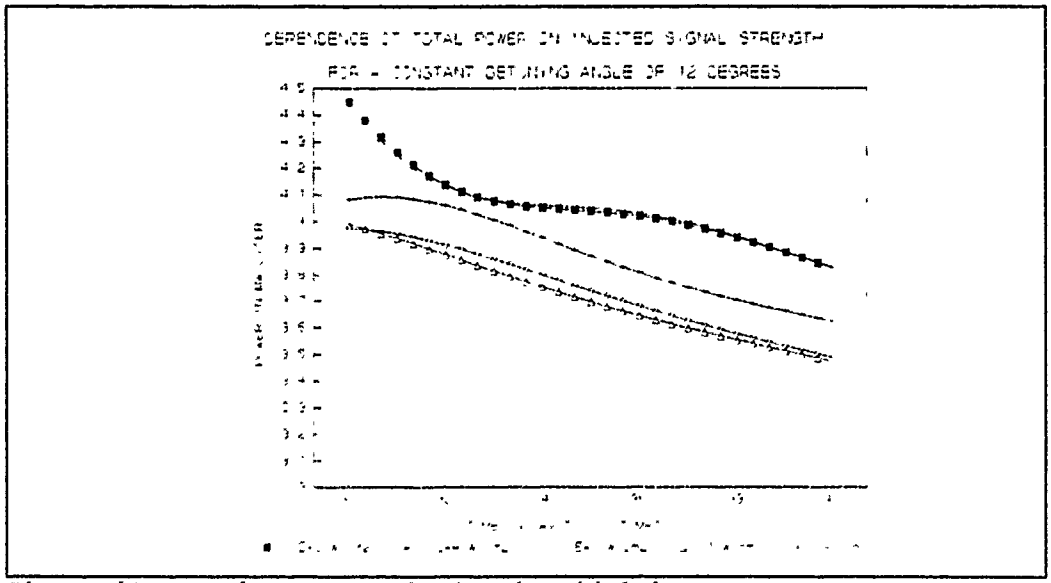

Figure 34 Total Power Evolution in Mid Pulse

As seen in Figures 32 through 34 for very low powers the effect on the total output is very small. At higher powers the injected signal has a dominant effect on the power evolution.

Behavior of Injected Signal at Various Detuning Angles

Lachambre found that the mode selection region was as large as 0.4π. This region decreased as the injected signal strength decreased. He also noted that the peak of the injected signal was retarded in time as the offset increased. This model predicts similar effects.

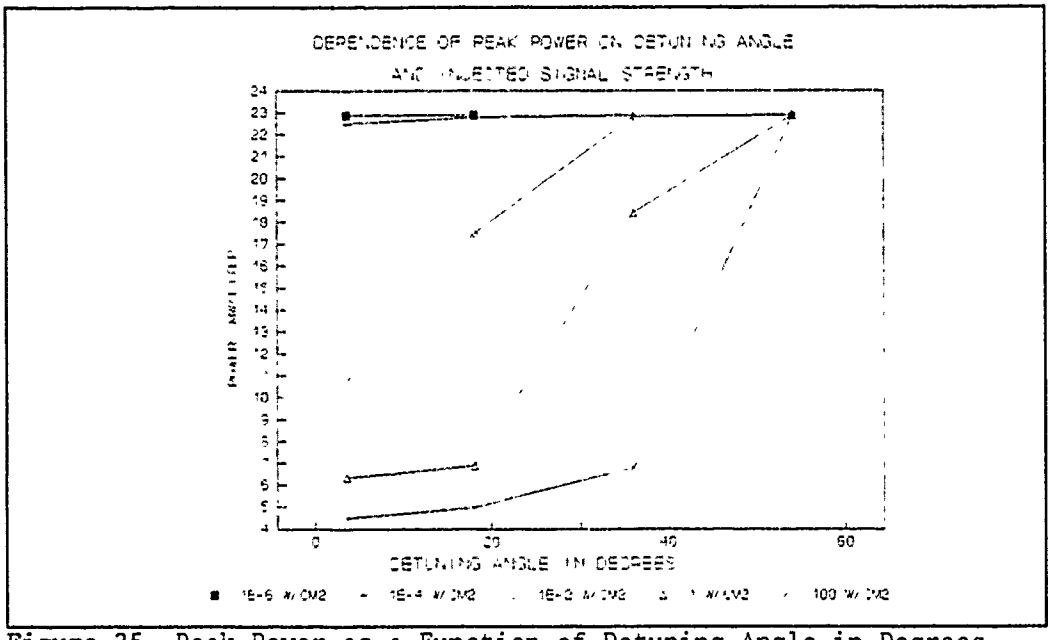

Figure 35 Peak Power as a Function of Detuning Angle in Degrees

Figures 35 through 38 are based on the output due to model running with Lachambre's parameters.

Table I Lachambre's Parameters

Active Length	= 1 meter	He	= .7 atmospheres
L_{res}	= 1.5 meters	CO_2	= .15 atmospheres
T	= 72%	N_2	= .15 atmospheres
R	= 28%	Volume	= 100 cm^3

In table I is the list of the applicable variables to the current model. T is the same value in Eq (13) of Chapter II. This is equal to (1-

β)/100 at the end of Chapter III. R is the reflectivity. The volume is translated into the area of the secondary mirror multiplied by the active section length. The partial components for the gases are translated into their appropriate fractions for use in the program. Figure 35 shows that the total peak power is very low for small detuning angles as much of the energy is consumed in the early degradation of the population inversion by the injection flux density. The power of the total combined flux densities reaches a plateau past 50 degrees. This implies that the injected signal is weak. This is indeed the case. The effect of the injected signal at large detuning angles is small. From Figure 13 Lachambre found little total energy contribution past 0.35π.

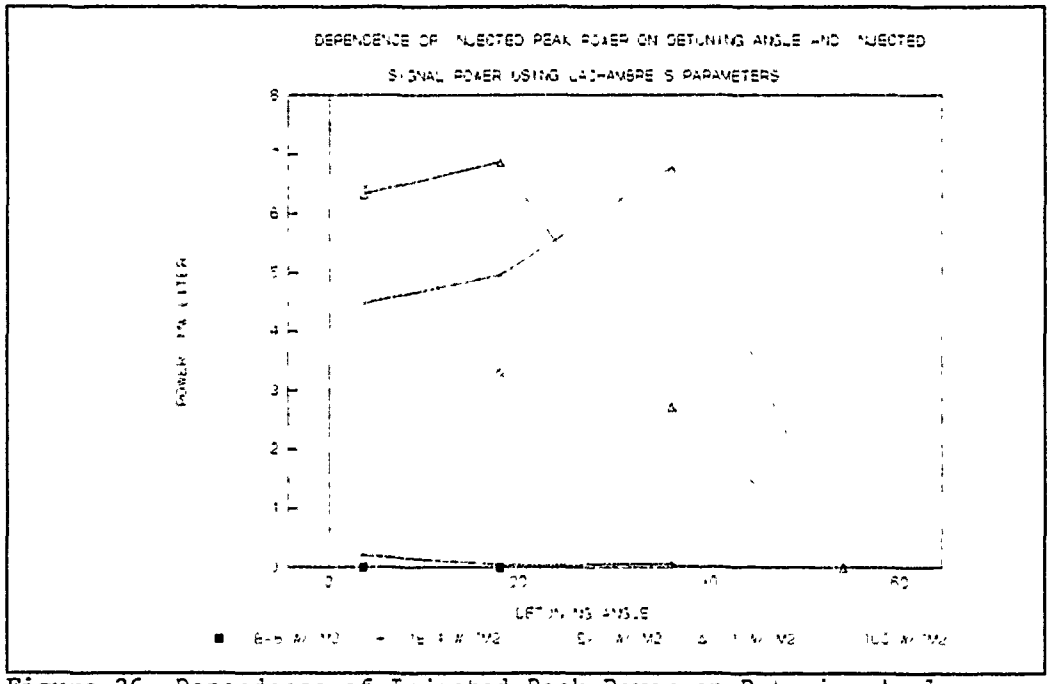

Figure 36 Dependence of Injected Peak Power on Detuning Angle

As seen in Figure 36, the injected signal dies quickly outside the mode selection range. The same effect is seen in the time of the power peaks. The smaller the injection detuning angle is the more effective the injected signal becomes at inducing a response. The injected peak power occurs earlier but the peak power is lower.

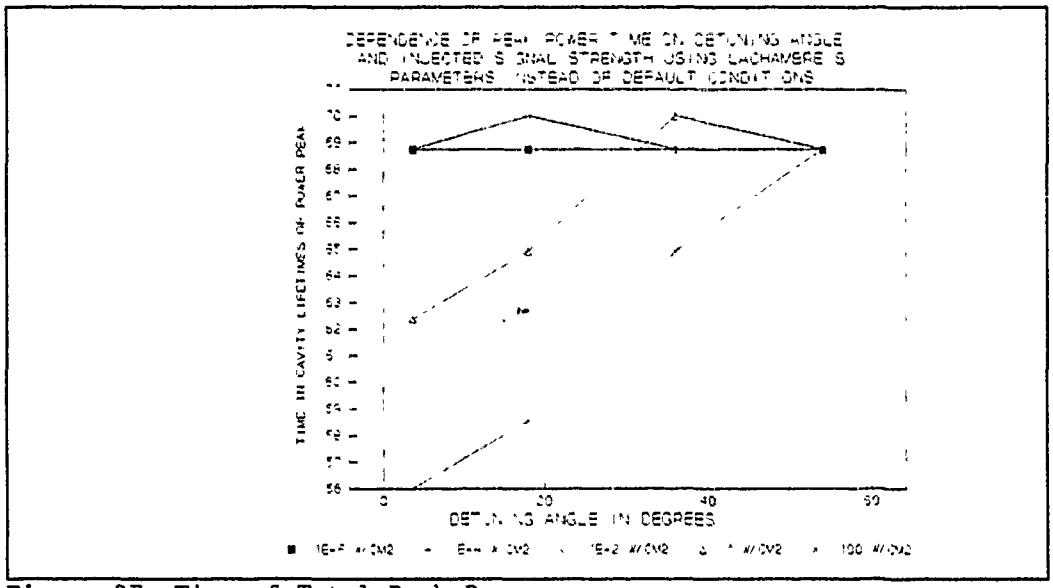

Figure 37 Time of Total Peak Power

As the injected signal power increases the peak power time decreases corresponding to the early depopulation of the inversion. The peak power occurs later as the detuning angle increases. This corresponds to a decrease in the effect by the injected signal. This effect plateaus in correspondence to the undriven case.

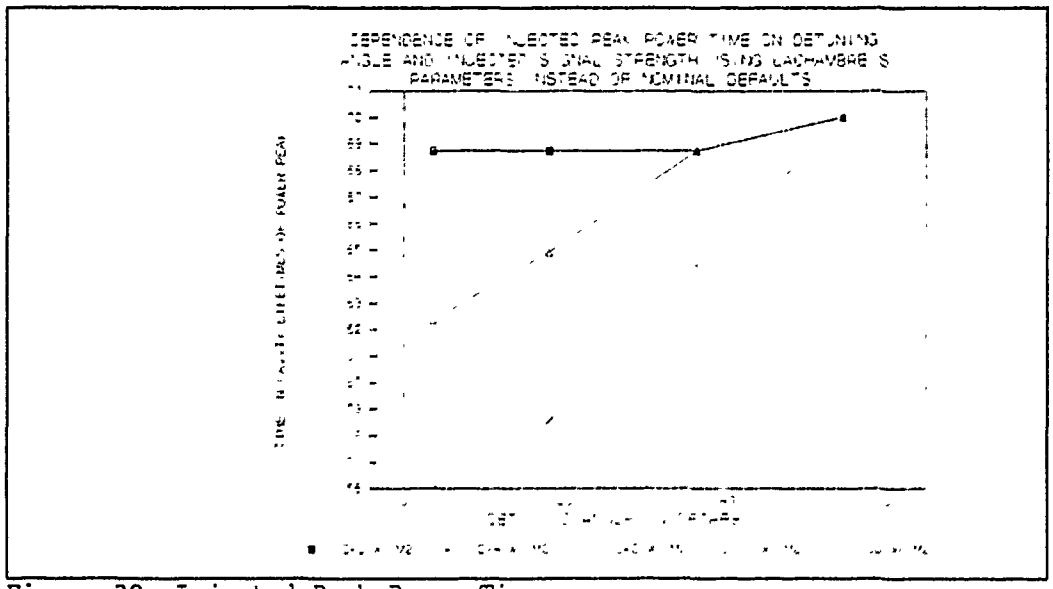

Figure 38 Injected Peak Power Time

Inside a limited range, the majority of a pulse's power comes from the injected signal. The proportion of the energy that is due to the injected signal is significant. However, the amount of the power due to injection decreases quickly as the size of the input signal decreases and the frequency offset from the nearest longitudinal mode increases.

Chapter VII Conclusion

Within the confines of the point model for the laser and the small signal approximation Lachambre's equations predict the behavior of injection mode locking in CO_2 lasers. There are three regimes of injection locking: a region at large detuning angles where the injected signal has little to no effect on the pulse forming process and contributes little to the total power; a region where the injected signal influences the power evolution of the cavity and enhances the output of the nearest longitudinal mode; and a region at extremely high power and small detuning angles where the laser will oscillate at the injected signal. Indications of injection mode selection are the oscillation of the phase in synchronous the initial cavity detuning angle. Symptoms of non-mode selection are the lack of contribution to the power output or early oscillation of the phase in the injected signal resulting in a beat frequency oscillation. In the mode selection regime phase tends to follow the rising gain. This makes sense when Eq (37) is examined in this new light. As the variable η grows larger, $d\theta/dt$ becomes simply the value of the detuning angle/time. When this is integrated over time the result is the detuning angle. Mode selection has little dependence on the nearest mode. The primary factors in determining mode selection are the detuning angle and the injected signal power in that order. Mode number is a distant third. Increasing the pressure will increase the gain and hence the output of the laser. Incorporating a reduced cavity length decreases the output power in an inverse manner - as the active section to cavity length ratio decreases the power output of the laser decreases.

Bibliography

1. Arfken, George. Mathematical Methods for Physicists (Third Edition). New York: Academic Press, 1985.

2. Cassard, Philippe and Jean-Michael Lourtioz. "Injection Locking of High-Power Pulsed Lasers - Part I: Monochromatic Injection." IEEE Journal of Quantum Electronics, 24: 2321-2337 (November 1988).

3. Gilbert, J. et al. "Dynamics of the CO_2 Atmospheric Pressure Laser with Traverse Pulse Excitation." Canadian Journal of Physics, 50: 2523-2535 (1972).

4. Glazenkov, V. M. et al. "Experimental Determination of the Parameters of Vibrational-Rotational Transitions in Isotropic Forms of CO_2 Molecules." Soviet Journal of Quantum Electronics, 18: 534-536 (April 1988).

5. Lachambre, J. L. et al. "Injection Locking and Mode Selection in TEA CO_2 Laser Oscillators." IEEE Journal of Quantum Mechanics, 12: 756-764 (1976).

6. Milonni, Peter W. and Joseph H. Eberly. Lasers. New York: John Wiley and Sons, 1988.

7. Nevdakh, V. V. "Spontaneous Emission Probabilities and Collisional Line Widths of 00°1 - [10°0, 02°0] Lasing Transitions in the CO_2 Molecule." Soviet Journal of Quantum Electronics, 14: 1091-1094 (August 1984).

8. Siegman, A. E. Lasers. Mill Valley, California: University Science Books, 1968.

9. Stone, D. Computer Code based on Gilbert's work. (1988)

10. Smith, Kenneth and R. M. Thompson. Computer Modeling of Gas Lasers. New York: Plenum Press, 1978.

11. Tratt, D. M. et al. "Spectral Control of Gain-Switched Lasers by Injection-Seeding: Application to TEA CO_2 Systems." Progress in Quantum Electronics, 10: 229-265.

12. Verdeyen, Joseph T. Laser Electronics. Englewood Cliffs, New Jersey: Prentice Hall, 1981.

13. Witteman, W. J. The CO_2 Laser. Berlin: Springer-Verlay, 1987.

REPORT DOCUMENTATION PAGE

Form Approved
OMB No. 0704-0188

1a. REPORT SECURITY CLASSIFICATION UNCLASSIFIED	1b. RESTRICTIVE MARKINGS
2a. SECURITY CLASSIFICATION AUTHORITY	3. DISTRIBUTION/AVAILABILITY OF REPORT Approved for public release; distribution unlimited
2b. DECLASSIFICATION/DOWNGRADING SCHEDULE	
4. PERFORMING ORGANIZATION REPORT NUMBER(S)	5. MONITORING ORGANIZATION REPORT NUMBER(S)
6a. NAME OF PERFORMING ORGANIZATION School of Engineering 6b. OFFICE SYMBOL (If applicable) AFIT/ENG	7a. NAME OF MONITORING ORGANIZATION
6c. ADDRESS (City, State, and ZIP Code) Air Force Institute of Technology (AU) Wright-Patterson AFB, Ohio 45433-6583	7b. ADDRESS (City, State, and ZIP Code)
8a. NAME OF FUNDING/SPONSORING ORGANIZATION 8b. OFFICE SYMBOL (If applicable)	9. PROCUREMENT INSTRUMENT IDENTIFICATION NUMBER
8c. ADDRESS (City, State, and ZIP Code)	10. SOURCE OF FUNDING NUMBERS PROGRAM ELEMENT NO. / PROJECT NO. / TASK NO. / WORK UNIT ACCESSION NO.

11. TITLE (Include Security Classification)
COMPUTER MODEL OF AN INJECTION LOCKED PULSED CO_2 LASER

12. PERSONAL AUTHOR(S)
Allen M. Susie Captain US Army

13a. TYPE OF REPORT	13b. TIME COVERED	14. DATE OF REPORT (Year, Month, Day)	15. PAGE COUNT
MS Thesis	FROM _____ TO _____	1990 December 1	68

16. SUPPLEMENTARY NOTATION

17. COSATI CODES			18. SUBJECT TERMS (Continue on reverse if necessary and identify by block number)
FIELD	GROUP	SUB-GROUP	Gas Lasers Mode Locked Lasers
09	03		

19. ABSTRACT (Continue on reverse if necessary and identify by block number)
MAJ David Stone

20. DISTRIBUTION/AVAILABILITY OF ABSTRACT ☒ UNCLASSIFIED/UNLIMITED ☐ SAME AS RPT ☐ DTIC USERS	21. ABSTRACT SECURITY CLASSIFICATION UNCLASSIFIED
22a. NAME OF RESPONSIBLE INDIVIDUAL Dr. David Stone MAJ USAF	22b. TELEPHONE (Include Area Code) DSN: 785-2012 22c. OFFICE SYMBOL AFIT-ENP

A homogeneously broadened CO_2 laser is examined as a point model with injection locking. Three distinct behavior regions are discovered in confirmation of previous works by Lachambre, Tratt, and Cassard. Low power injection at medium-to-low offtuning angles causes the nearest longitudinal mode to dominate all other modes. High power injection at very low offtuning angles causes the injection signal to amplifiy and dominate all of the longitudinal modes. The injected signal has little effect on the power or energy evolution of the multimode cavity at large offtuning angles. A computer model written in QuickBASIC© for use on an IBM-PC/AT© or compatible is used to examine the behavior of injected signals. Field and photon density rate equations are shown equivalent. The mixed flux-population equations are valid within the confines of the point model.